CHUARIA, *VENDOTAENIA*, AND THE TAPHONOMY OF THE CARBONACEOUS COMPRESSION

Evan Pelzner Anderson

Thesis submitted to the faculty of the Virginia Polytechnic Institute and State University in partial fulfillment of the requirements for the degree of

Master of Science
In
Geosciences

Shuhai Xiao, Chair
Michal J. Kowalewski
J. Fred Read

May 3, 2010
Blacksburg, VA

Keywords: *Vendotaenia*, *Chuaria*, Carbonaceous Compression, Taphonomy, Elemental Mapping

CHUARIA, *VENDOTAENIA*, AND THE TAPHONOMY OF THE CARBONACEOUS COMPRESSION

Evan Pelzner Anderson

ABSTRACT

Carbonaceous Compressions are a widespread preservational style for fossils, yet their taphonomy remains poorly understood. Previous studies focusing on the taphonomy of carbonaceous compressions have primarily looked at exceptionally preserved faunas in plane view. The precious nature of these fossils leaves destructive techniques of analysis out of the question, but these techniques are necessary if the taphonomy of carbonaceous compressions is to be deciphered. This study analyzes Neoproterozoic carbonaceous compressions from the Yangtze Gorges area in order to address this issue. *Chuaria* fossils from the Jiulongwan, Sixi, and Sifangtan sections of the Doushantuo Formation and *Vendotaenia* fossils from the Wuhe and Miaohe sections of the Denying Formation are microchemically analyzed in both plane view and cross section in order to gain a greater understanding of the makeup of carbonaceous compressions. Results confirm and elaborate on previous studies. Likely clay coats are detected on some *Chuaria* specimens, while they are absent on less thermally mature specimens. Evidence for sulfate reduction in association with carbonaceous compressions is found. Sulfur enrichment, rather than clay coats, is found in association with *Vendotaenia* fossils. These observations lead to the hypothesis that while organic remains require a very precise set of taphonomic conditions in order to be preserved as carbonaceous compressions, there may be more than one set of conditions that allow for preservation. More studies of a greater taxonomic and taphonomic range of carbonaceous compressions are needed, however, if the mechanisms which control this preservational pathway are to be fully understood.

ACKNOWLEDGMENTS

My time at Virginia Tech has been a whirlwind tour, but even so, I am amazed at how much I have learned and grown in just the short amount of time I have been here. First to thank is my advisor, Dr. Shuhai Xiao, for introducing me to both geochemistry and taphonomy, and opening to me a world of paleontology I scarcely knew existed. Without his guidance and help, this project would never have even gotten off the ground. I also wish to thank my other committee members Dr. Michal Kowaleski and Dr. J. Fred Read for their input into this project, and their patience when it comes to a person who so often takes just a little too long to get things done. Of course, I wish to thank my parents, Kathleen and Laurence Anderson, for the constant moral support throughout my time here, and being there for me wherever, whenever, no questions asked. I also have to thank Jim Schiffbauer for dealing with my constant barrage of questions regarding academic matters, and for showing me the ropes with elemental mapping. I also must thank Steve McCartney for teaching me how to operate an ESEM at the Virginia Tech Institute for Critical Technology and Applied Science Nanoscale Characterization and Fabrication (ICTAS-NCFL), where I actually wound up collecting my whole data. And I must thank all my fellow grad students in the Geoscience Department, particularly my officemates this past year, Mike Meyer and Jackie Wittmer, and Tina Blue and JoBeth Carbaugh from the realm of sedimentology downstairs, who helped me to enjoy my time here and keep me sane when the academic pressure was on.

TABLE OF CONTENTS

LIST OF FIGURES

LIST OF TABLES

INTRODUCTION

Carbonaceous compressions are a common and important constituency of the fossil record. This taphonomic style preserves the original (although keroginized) carbon of a 3-dimensional organism as a 2-dimensional compression onto a layer of sediment. It is a common mode of preservation for organisms as disparate taxonomically as graptolites and metaphytes, and as distant temporally as Eocene insects and microscopic carbonaceous compressions dating back to the Archaean (Javaux, 2010). However, the taphonomy of carbonaceous compressions remains poorly understood. One of the more vexing problems concerns their secular distribution throughout the marine fossil record. Carbonaceous compressions were common throughout the Proterozoic, reached a spectacular climax of preservational quality from the Neoproterozoic to middle Cambrian, and then began to become increasingly rare in the marine realm thereafter (Butterfield, 1995)

Among the organisms that are preserved as carbonaceous compressions are the spectacular Cambrian fossils of the Burgess Shale, Maotianshan Shale, and Wheeler Shale (Butterfield, 1990; Aronson, 1992; Butterfield, 1995; Orr, 1998; Gabbot, 2004; Butterfield, 2007; Gaines, 2008; Page, 2008). Thus far, most analytical attempts to understand the taphonomy of carbonaceous compressions have revolved around these instances of exceptional preservation. However, since the basic taphonomic pathway between more common carbonaceous compressions, such as *Vendotaenia* and *Chuaria*, and exceptionally preserved fauna like the Burgess Shale is the same (Butterfield, 1995; Gaines, 2008; Page, 2008), resolving the taphonomy of the former, invasively if necessary, can provide insights into the latter. This study does just this, by looking at the preservation of *Chuaria* from the Doushantuo Formation and *Vendotaenia* from the Denying Formation, both exposed in the Yangtze Gorges area of

South China. By examining carbonaceous compressions in both plane view and cross section we are able to provide insights into the taphonomy of carbonaceous compressions hitherto unavailable. Through the use of light microscopy, scanning electron microscopy, Raman spectroscopy, and Energy Dispersive X-Ray Spectroscopy (EDS), we here present information on the distribution of elements in carbonaceous compressions, as well as information on the organic maturity and three-dimensional structure of the compressions.

BACKGROUND

History of the Carbonaceous Compression

Butterfield (2003) listed six basic kinds of exceptional preservation from the critical Neoproterozoic-Phanerozoic transition, and detailed both the preservational advantages and limitations of the various taphonomic pathways. Among these he included the Burgess Shale-type preservation, where the original keroginized carbon of an organism is preserved as a two-dimensional compression, generally in fine grained sediments. As established by Page et al. (2008) and Gaines et al. (2008), Burgess shale-type preservation is the same basic taphonomic pathway as those of Proterozoic organic-walled compression fossils. Thus, we shall hereafter refer to the preservation of all such organisms preserved as organic-walled fossils as carbonaceous compressions. In the case of exceptionally preserved carbonaceous compressions, as those typifying the Burgess Shale and Chengjiang faunas, we will term them exceptional carbonaceous compressions.

The carbonaceous compression taphonomic pathway has been known for some time, with a large number of Proterozoic taxa known only from this preservational style (see Hoffman [1994] for an overview of Proterozoic carbonaceous compressions). The intense study that has highlighted the past fifteen years of research into carbonaceous compression taphonomy did not begin until Butterfield (1990) identified fossils from the Burgess Shale as carbonaceous in composition through isolation via HF maceration. This was an unexpected development to much of the paleontological community. Allison (1988) did not even consider carbonaceous compressions in his review of exceptional fossil preservation taphonomies. However, once the discovery was made an explanation was sought as to how such a high amount of anatomical detail could be preserved through organic preservation alone (Briggs, 1994). Particularly

intriguing was the observation that Burgess-Shale type preservation became very rare in the marine realm after the Cambrian (Aronson, 1992). While it is true the carbonaceous compression taphonomic pathway did not disappear after the Cambrian—graptolites are preserved as carbonaceous compressions and are one of the most ubiquitous deep water fossils of the Ordovician and Silurian—after the middle Cambrian it became extremely unusual to find such taxonomic groups as polychaetes and priapulids preserved as carbonaceous compressions in marine sediments (Butterfield, 1995). The lack of an actualistic environment present in the modern marine realm made determining the taphonomy of carbonaceous compressions particularly difficult.

What was apparent was that if relatively fragile organic tissue was to be preserved as exceptional carbonaceous compressions without the aid of permineralization or authigenic mineralization (Briggs, 2003), some mechanism, or set of mechanisms, must be responsible for the delay of the degradation of the organic material until it is buried to great enough depth to be protected from further biologically-mediated decay. This mechanism would have to slow both aerobic and anaerobic decay; for while anoxic conditions will certainly slow down the decay of a carcass, given sufficient time and electron acceptors, anaerobes are capable of completely degrading an organism's remains.

An early hypothesis held that a simple increase in bioturbation would be sufficient to remove exceptional carbonaceous compressions from the fossil record. Bioturbation, after all, increases the flow of oxygen into sediments, increasing aerobic degradation of dead organisms buried in the sediments, and provides greater access to other chemical species for anaerobes (Orr, 2003). This hypothesis was questioned by Aronson (1992) when he showed that only an unrealistic increase in bioturbation depth and intensity after the Cambrian could account for the

paucity of post-Cambrian exceptional carbonaceous compression deposits in the Paleozoic. While his analysis was done in an attempt to demonstrate that the disappearance of some of the more unusual faunas found in the Burgess Shale was not simply due to taphonomic overprinting, his study and later considerations (Allison, 1993; Aronson, 1993) demonstrated that increase in bioturbation alone could not have accounted for the decline of exceptional carbonaceous compressions. A later study by Orr et al. (2003) considered the possibility that increases in specific ethologies of bioturbation could at least partly account for the disappearance of exceptional carbonaceous compressions. They demonstrated a post-Cambrian increase in particularly invasive ethologies of bioturbation, such as agrichnia and fodichnia, and a statistically significant increase in bioturbation after the Cambrian in deep-water marine environments that hosted exceptional carbonaceous compressions.

While Orr et al. (2003) considered the consequences of a broken permeability seal on the efficacy of exceptional carbonaceous compressions, Gaines et al. (2005) looked at the establishment of a permeability seal for the preservation of Burgess-Shale faunae in the Wheeler Shale of Utah. They postulated that limited sulfate reduction of carbonaceous compressions would produce hydrogen sulfide, which, combining with pore waters to form sulfuric acid, would dissolve the surrounding partly micritic matrix. After carbonate ions migrated away from the zone of sulfate reduction, they would precipitate as a seal of permeability-blocking calcite crystals. This seal would then have suffocated the anaerobic bacteria by denying them sulfate from the overlying water column.

What both hypotheses failed to consider, however, was a third degradation path which must also be slowed in order for organic matter to be preserved: that of autolytic decay (Allison, 1988; Butterfield, 1990; Butterfield, 1995). All organisms contain enzymes which are meant to

help degrade their cells and organelles in a controlled manner; this is necessary for an organism's continued maintenance and growth. However, upon death, these enzymes become unconstrained and break down the structure and detail of the decaying organism. Even in the absence of aerobic and anaerobic bacterial decay, complete and total tissue degradation may proceed in a matter of days only from autolytic decay (Allison, 1988; Butterfield, 1995). Butterfield (1990, 1995) considered the possibility of the slowing and deactivation of autolytic decay due to bonding between autolytic molecules and highly reactive clay molecules, such as smectites rich in monovalent cations like sodium. For autolytic inhibition by absorption on clay minerals to be effective a set of chemical requirements must be met, including specific pH, usually in the range of 4 to 5 (Butterfield, 1990). This allows for the residual charge on clay minerals and enzymes to be opposite. There must also be a large proportion of clay particles to organic matter, or else the sheer number of organic molecules will overwhelm the clay minerals' ability to bind or deactivate the decaying organism's enzymes (Butterfield, 1995). This makes for a hypothesis that is difficult to prove, as the clays that suppress or inactivate the enzymes are among the most unstable clays, and the first to be diagenetically altered. Thus, direct evidence of such clays would be difficult to find, particularly in Proterozoic to early Paleozoic rocks.

Although the original enzyme-deactivating clays may not be preserved, Orr et al. (1998) found evidence for an aluminosilicate coating on a carbonaceous compression of *Marella splendens*. Remarkably, not only did the *Marella* show a relative enrichment in elements such as silicon, aluminum, and iron, but also certain enrichments seemed to correspond with different anatomical features. For example, the outer cuticle of the animal was marked by relative enrichment in silicon, while the intestinal tract was marked by a relative enrichment in potassium and aluminum. Orr et al. (1998) contended that the clay particles physically adhered to the

tissues and exoskeleton of the animal during early decay, and served to protect and mold the arthropod, preserving the original outline and structural detail. They attributed the different elemental composition of the clays adhering to *Marella* to the timing of decay: the more labile, chitinous lining of the gut (Butterfield, 1990) would have decayed earlier and attracted more chemically reactive clays, whereas the more recalcitrant outer cuticle would decay later, attracting more stable clays. Alternatively, the relative enrichment in certain elements could have come from the tissues of the animal itself. This discovery proved to have utility as well: the putative lobopod limbs of *Opabinia regalis* were demonstrated to be more parsimoniously interpreted as pleural extensions of the alimentary canal, since the "limbs" and the guts shared the same elemental enrichments (Zhang, 2007).

The discovery of Orr et al. (1998) raised the possibility that although carbonaceous compressions might not be wholly authigenically mineralized (Allison, 1988; Briggs, 2003), it might not be possible to fossilize a carbonaceous compression without partial authigenic mineralization. Indeed, Gabbot et al. (2004) demonstrated through Scanning Electron Microscopy analysis that most "carbonaceous compressions" of the Chengjiang Biota of the Maotianshan Shale were made of 1.25-14 μm wide iron oxide crystals. These crystals were pseudomorphs after framboidal, cubical, and even octahedral pyrite. In only one specimen was point elemental analysis able to detect a relative enrichment of carbon. However, if sufficient weathering had occurred in the Maotianshan Shale for pyrite to oxidize into iron oxide, it would not be surprising that organic carbon in the carbonaceous compressions was oxidized and mobilized as well (Butterfield, 2003; Gabbot, 2004; Gaines, 2008).

A reexamination of the Burgess Shale itself by Butterfield et al. (2007) began to lead to our present understanding of carbonaceous compression taphonomy. They observed that not

only were carbonaceous compression fossils coated with aluminosilicate minerals, as Orr et al. (1998) had found, but also aluminosilicates had partially or completely replaced the tough calcite sclerites of *Olenoides* and diagenetic veinlets of calcite running through the rock. They took this as strong evidence that the "clay coats" were late diagenetic in origin, and not of direct importance to the preservation of the carbonaceous compressions. Page et al. (2008) corroborated this evidence by showing that aluminosilicate films on graptolites and those on non-mineralizing arthropod cuticle from the Burgess Shale were both coincident with the carbonaceous material, or surrounded it. In addition, they observed that the thickness of associated aluminosilicate films increased in both graptolites and arthropods with an increase in the degree of diagenetic/metamorphic alteration of the host rock. Like Orr et al. (1998), Page et al. (2008) also found different anatomical structures to have different aluminosilicate film compositions. Graptolite periderm tended to have aluminosilicates with a chloritic and illitic composition. Arthropod cuticle tended to be illitic in composition, whereas arthropod "soft-parts" were illitic or kaolinitic in nature. These enrichments were not diagnostic, however, and varied from sample to sample. Page et al. (2008) hypothesized that the variation in aluminosilicate mineralogy reflects the different phylloscilicates that were stabilized during progressive diagenesis and metamorphism.

Gaines et al. (2008) contended that both the Burgess Shale and Maotianshan Shale are not the optimum examples to understand the taphonomy of carbonaceous compressions due to the metamorphism of the former and heavy weathering of the latter. Instead, they made elemental maps of numerous carbonaceous compressions from other, less diagenetically altered sites from the Proterozoic, Cambrian, and Ordovician. In all cases, they found a relative enrichment of carbon; at times they even discovered carbonaceous films through EDS mapping

that were not noticeable in visible light. This led them to the conclusion that carbonaceous compressions essentially share the same taphonomy as flattened carbonaceous material derived from tissues, cell walls, and encystments. Thus, this united the carbonaceous compressions of Proterozoic algae and Paleozoic graptolites with the "Burgess-shale type" compressions.

Although many questions surrounding carbonaceous compressions have been answered in recent years, there are still many unresolved issues. Critically, no comprehensive model has yet been proposed relating observed taphonomic characteristics of carbonaceous compressions with the need to slow degradation due to aerobic microbes, anaerobic microbes, and autolytic decay via various proposed mechanisms, including permeability sealing, a lack of bioturbation, anoxia, and the adherence of highly reactive clays to organic substrates (Butterfield, 1990; Allison, 1993; Butterfield, 1995; Orr, 1998; Briggs, 2003; Chin, 2003; Orr, 2003; Gabbot, 2004; Gaines, 2005; Butterfield, 2007; Gaines, 2008; Page, 2008).

A good first step would be to resolve the three-dimensional placement of the aluminosilicates and/or pyrite associated with the carbonaceous compressions. Several physical configurations relating aluminosilicate coats to carbonaceous compressions have been proposed (Orr, 2009), but so far Butterfield et al. (2007) have been the only ones to test these configurations through elemental mapping of carbonaceous compressions in cross section. This study fills this gap by looking at the cross-sectional elemental distributions of two ubiquitous carbonaceous compressions, *Chuaria* and *Vendotaenia*, that have been somewhat neglected in the recent work on carbonaceous compression taphonomy. However, before the results, implications, and limitations of this study can be discussed, a review of the morphology, taxonomy, and historical treatment of *Chuaria* and *Vendotaenia* is in order.

Chuaria *and* Vendotaenia *as carbonaceous compressions*

Chuaria and *Vendotaenia* are generally not considered to be true genetic taxa, but are instead form taxa (Steiner, 1996) diagnosed by relatively few, but distinctive, characteristics. *Chuaria*, as typified by its type species *C. circularis*, is a circular, originally spherical organic-walled vesicle anywhere between 400 microns and 5 mm in diameter. It is relatively thick walled (more than 2 microns) and lacks any surficial ornamentation, save concentric circles or arcs which form as a consequence of compression (Steiner, 1996). *Chuaria* is most often preserved as a carbonaceous compression (e.g.(Kumar, 2001; Samuelsson, 2001), but can also be preserved three-dimensionally through pyritization (Yuan, 2001), and in chert nodules through silicification (Steiner, 1996).

Chuaria occurs throughout the Proterozoic, but it forms a distinctive association with *Tawuia* in the Neoproterozoic (Hoffman 1994). This has lead some authors (e.g.(Kumar, 2001) to suggest that *Chuaria* and *Tawuia* are intimately related, as separate stages in a life cycle or different parts of the same organism. Regardless, most authors consider *Chuaria* to be a eukaryotic alga, although the detail of preservation has never been good enough to allow assignment to any one group. Steiner (1996), however, thought *Chuaria*'s incredibly variable size and shape to be atypical for a eukaryotic alga, and determined *Chuaria* to be a prokaryotic colony, perhaps of cyanobacteria. Most workers admit, though, that what is called *Chuaria* actually encompasses many different taxa of different phylogenetic affinities at different stages of their life cycle (Hofmann, 1994; Steiner, 1996; Yuan, 2001; Xiao, 2002), and the designation under the name *Chuaria* or more general "chuarid" is a taxonomic convenience for a group of fossils that look remarkably the same.

In a similar situation is *Vendotaenia*, a fossil characterized by its ribbon shape, occasional longitudinal striations, and spheroidal structures on the ribbon in exceptionally preserved specimens (Vidal, 1989; Hofmann, 1994). Like *Chuaria*, its geologic range runs from the Paleoproterozoic to the Neoproterozoic (Hoffmann, 1981; Hofmann, 1994). *Vendotaenia* is made of more robust and more easily preserved organic material relative to most other Neoproterozoic carbonaceous compressions. *Vendotaenia* does resemble some very elongate *Tawuia* (Kumar, 2001), but *Vendotaenia* has sharp and rectangular, rather than rounded, terminations. Like *Chuaria*, *Vendotaenia* has unknown taxonomic affinities. In particular, the spheroidal structures present in some specimens have tempted comparison to algae sporangia, but Vidal (1988) offered an alternative interpretation as an oversized sheath protecting sulfur oxidizing bacteria colonies. However, given its variable size, appearance, and chronologic range it is entirely possible that *Vendotaenia* represents multiple phylogenetic taxa.

In spite of their uncertain phylogenetic affinity and variable preservational quality, *Chuaria* and *Vendotaenia* both are very robust carbonaceous compressions, and occur abundantly in many formations in the Neoproterozoic. It is for this reason that this study has chosen these two taxa to stand in as archetypes, as it were, for carbonaceous compressions on the whole. Their abundance means that any destructive techniques applied to them are of little consequence, which is a distinct advantage over studying precious taxa for which there may be only a few representatives, as can be the case for exceptional carbonaceous compressions.

MATERIALS

The fossils used for this study come from the Doushantuo and Denying formations exposed near the southern end of the Huangling Anticline in the Yangtze Gorges area, Hubei Province, South China (Figure 1). The Doushantuo and Denying formations of this area were deposited in a shallow, often restricted, intra-cratonic basin on the Yangtze platform (Wang, 1998; McFadden, 2008; Ader, 2009) and contain abundant carbonaceous compression fossils, including the exceptional carbonaceous compression Miaohe biota from the uppermost Doushantuo Formation (Fig. 1; (Xiao, 2002).

The relatively shallow nature of the basin is evident in the distribution of facies within the Doushantuo and Denying Formations (Fig. 2A). The Doushantuo is often divided into four informal lithostratigraphic members. All four are present in two of the examined sections: the Sixi and Jiulongwan, while only the first three are present at the Sifangtan section. Member I is the cap carbonate overlying the Nantuo Diamictite and is around 5 m thick (Wang, 1998). Member II is 70 to 100 m thick and consists of alternating beds of argillaceous dolomitic pelletal packstones and calcareous siltstones with numerous chert nodules which contain exceptionally preserved microfossils. The lithologic proportions of packstones to siltstones increase upsection, which is usually interpreted as representing a shallowing trend for the basin at this time. The contact between Member II and III is lithologically subtle, and is evidenced by the appearance of sheet cherts and an overwhelming abundance of dolomitic pelletal packstone. Member III ranges from 50 to 80 m in thickness, depending on locality, and can contain scours, microbial laminites, graded beds, and breccia beds (McFadden, 2009). Member IV is a unit of organic rich mudstone and siltstone from a few meters to 20 m thick. The famous Miaohe biota is found within this member at the Miaohe site. *Chuaria* specimens were collected for this study from the calcareous

siltstone of Member II at the Jiulongwan locality (Fig. 1) by Lin Dong in 2005 and the author and his companions in 2009. Additional *Chuaria* specimens, primarily from the argillaceous packstone of upper Member II, were collected from the Sixi section by Shuhai Xiao in 2008 and the author and his companions (including SX) in 2009. Finally, some small size mini-chuarids, hereafter called small *Chuaria*, were also collected by the author and his companions in 2009 from Member II at the Sifangtan and Jiulongwan localities.

The Denying Formation consists of three members in the southern Huangling Anticline (Wang, 1998): the basal Hamajing Member, a 20-190 m thick light gray dolostone unit which is in places karstified, the 100-160 m thick Shibantan Member, which consists of dark gray, recrystalized bituminous limestone interbedded with laminae of siltstone; and the Baimatuo Member, a 60-570 m thick unit characterized by light gray, massive, heavily recrystallized and karstified dolostone. *Vendotaenia* fossils occur in siltstone beds of the Shibantan Member. Material for this study was collected from the Wuhe Section in 2003 (Shuhai Xiao) and the Miaohe and Wuhe sections in 2009 (Evan Anderson).

METHODS

Methods used for this study encompass both traditional observational methods and more advanced tools in order to reveal the maximum amount of information possible on analyzed specimens. Collected samples were isolated into small chips and observed through a dissecting microscope to identify areas of interest for further study. Selected samples were cut up and prepared for thin sectioning perpendicular to bedding planes. To ensure maximum likelihood that an observed carbonaceous compression was in fact a *Chuaria* or *Vendotaenia* fossil, whenever possible thin sections were cut perpendicular to a bedding plane which could be observed to contain dense populations of fossils. Once made, thin sections were examined under both a dissecting microscope and a transmitted light petrographic microscope to observe sedimentary composition of the matrix, and to locate and identify *Chuaria* and *Vendotaenia* specimens.

Selected *Chuaria* and *Vendotaenia* specimens in both thin sections and on isolated chips were imaged and analyzed using a FEI Quanta 600F ESEM. Images were taken in Secondary Electron (SE) and Back Scattered Electron (BSE) modes at either 20 or 12 kV, spot size 5 to 6. In order to improve conductance, a gold-palladium coat was applied to isolated chip samples with a Cressington Sputter Coater HR to a thickness of 19.9 to 20.2 nm. Thin sections were sputter coated to a thickness from 7.6 to 8.0 nm. Once imaged, a Bruker Advanced X-ray Solutions Quantax energy dispersive X-ray spectrometer (EDS) was used for point analysis of elemental compositions and for generating elemental maps of the fossils. It should be cautioned that analyses done with the EDS are semi-quantitative in nature: they do not measure absolute elemental abundance. This is particularly true of elemental maps, which present elemental

abundances as monochromatic images where the saturation of the color hue is adjusted to match the range of the element's abundance in the mapped area. Thus, the saturation of the hue partly depends on the element's abundance in the matrix. Point elemental analyses are somewhat more quantitative, but the elemental abundances, returned as percentages, can really only be applied for the region of the sample from which the point analyses were taken. In spite of these limitations, confirmatory techniques used in conjunction with elemental mapping and point analysis can allow EDS to be a useful tool.

Chips bearing carbonaceous compressions, including *Tawuia*, *Chuaria*, and *Vendotaenia* specimens, were analyzed for organic carbon maturity using a JY Horiba LabRam HR800 Raman spectrometer with an Andor electronically cooled CCD detection system (1024x256). Analysis was performed using a Modu-Laser 100 mW 514 nm Ar laser with 600 grating. For this study, it was used to confirm that carbon enrichments observed in elemental mapping were indeed organic carbon. Raman spectroscopy was also used to estimate the thermal maturity of carbonaceous material.

Biometric analysis was done for *Chuaria* and small *Chuaria* from the Sixi, Jiulongwan, and Sifangtan sections to ascertain whether or not they came from the same population. Since most *Chuaria* are slightly elliptical, two axis measurements were taken for the fossils: the first axis was the longest length possible for the fossil. The second axis was measured at a 90° angle to this first. These lengths were log transformed to reduce skewness in the distribution of the samples. The log transformed area of each individual fossil was then calculated, and statistical tests were applied to the log transformed areas of the samples to test if they were significantly different from one another. Axes were measured on digitally captured photographs using Adobe Photoshop Elements 2.0 and ImageJ, and were statistically analyzed using JMP 8.0 and PAST.

DATA

Chuaria *from the Sixi and Jiulongwan sections*

The sedimentology of the examined portions of the Sixi and Jiulongwan sections is similar to what has been reported previously (Wang, 1998; McFadden, 2008) The Jiulongwan section has a predominance of the calcareous siltstone facies, and carbonaceous compressions from this lithology are uncommon to rare, consisting mostly of *Chuaria* compressions, broadly oval *Tawuia* compressions, and amorphous sheets of carbonaceous material, most likely bacterial mats. At the Sixi section *Chuaria* fossils are primarily concentrated in the argillaceous dolostone layers, and are common to abundant in many layers (Fig. B). The fossil assemblage consists almost entirely of *Chuaria*, although some lozenge shaped carbonaceous compressions and larger chuarid-like compressions can be found as well. Beds containing *Chuaria* are usually associated with large numbers of phosphatic grains (Figs. 3, 4 A-B), often as a layer of phosphate surrounding a core of silica (Fig. 4 B-C). The phosphatic grains are either disseminated throughout the matrix, or concentrated into what appear to be small lag deposits in the argillaceous dolostone laminae (Fig. 3B).

The *Chuaria* fossils themselves are easily seen on the bedding planes in most cases (Fig. 5A-B), except where highly weathered (Fig. 5C). This visibility is not apparent in secondary electron (SE) imaging on the ESEM due to a lack of topographic relief, but in backscattered electron (BSE) mode the low Z number of the carbon allows for the *Chuaria* specimens and other carbonaceous materials to be highly visible (Fig. 5D).

Despite the differing lithologies between the argillaceous dolostone at the Sixi section (e.g. Fig. 6A) and calcareous siltstone at the Jiulongwan section (e.g. Fig. 7A), elemental mapping found the chemical enrichments in *Chuaria* fossils from both localities to be very similar. Bedding plane elemental maps of a *Chuaria* specimen (08-SX-DST3-31b-#1) from the Sixi argillaceous dolostone reveal an enrichment in aluminum, magnesium, and silicon in the fossil (Fig 6D-F), and a depletion of calcium relative to the background (Fig. 6G). Carbon in the fossil is indistinguishable from the matrix carbon (Fig. 6H), which is not unexpected given the high carbon content of the dolomitic matrix. Similarly, A *Chuaria* specimen (JLW-27Af-#1) from the Jiulongwan section shows relative enrichments in aluminum, magnesium, and silicon (Fig. 7B-D) and concurrent depletion in calcium (Fig. 7E). There is little difference between matrix and fossil in carbon enrichment (Fig. 7F), much like the analyzed *Chuaria* specimen from argillaceous dolostone at Sixi.

Analysis shows weathering has a prominent role in what elements are detected in the carbonaceous compressions. Sample 09-SX-DST-F was collected from a calcareous siltstone bed at the Sixi section (Fig. 2B). Two specimens of *Chuaria* are located on the sample (Fig. 8): one had been exposed on the outcrop, while the other had been freshly revealed during sample preparation. The fresh *Chuaria* specimen (09-SX-DST-F-#1), seen as a slightly darker, smooth patch in BSE mode in Fig. 9A, contains relative chemical enrichments similar to other *Chuaria* specimens analyzed from the Jiulongwan and Sixi sections (Fig. 9C-I). On the other hand, the weathered *Chuaria* specimen (09-SX-DST-F-#2) appears in BSE mode images as a much darker area relative to the matrix, indicative of a low Z element (Fig. 10A-B). This corresponds to a relative enrichment of carbon (Fig. 10G). The relative enrichment of aluminum, magnesium,

and silicon seen in the weathered *Chuaria* specimen's companion is not observed here (Fig. 10-C-E).

Similarly, a *Tawuia* specimen (JLW-18F-#1) from the Jiulongwan section shows the effects of weathering. The large fossil is conspicuous in visible light (Fig. 11A), and can also be seen dimly in BSE mode (Fig. 11B). However, elemental analysis of the fossil shows that it is all but indistinguishable from the background (Fig. 11C-G). The fossil is distinguishable in visible light, so there must still be some residual material present. However, these materials must have elemental concentrations that are indistinguishable from the matrix.

Whereas in plane view *Chuaria* is quite conspicuous to visual inspection, their compressed nature makes them difficult to pick out in cross-section. Photographs of cross-sections under the dissecting microscope reveal thin black laminae, sometimes with a reflective film on the interior of the compression (Fig. 12A). More often even the more conspicuous cross-sections of *Chuaria* would appear as just a thin, solid black line (Fig.12C). Thin sections of the carbonaceous compressions reveal a translucent material surrounding the *Chuaria* fossils with enigmatic optical properties. They have a brownish appearance in plane polarized light, but exhibit very intense pleochroism from light brown to black with every rotation of the stage by 180° (Fig. 13B-C). Under cross polarized light, the compressions undergo extinction. The translucent habit of the carbonaceous compressions was visible even for extremely thin samples (Fig. 12B). Elemental mapping revealed that the translucent brown material is not carbon, but a material enriched in silicon, magnesium, and aluminum, just as had been observed in *Chuaria* fossils in plane view. An elemental map of a cross section of a large specimen of *Chuaria* (08-SX-DST3-3D1e-#1; Fig. 13A) shows a thin film, enriched in magnesium and silicon elements (Fig. 13E-F) surrounding a bulging core rich in calcium and phosphorous (Fig. 13G-H). Unlike

the carbonaceous compressions observed in plane view (Figs. 6H, 7F, 9G, and 11G), enrichment of carbon associated with the compression is present, but it is not visible at the magnification of Fig. 13I. A higher magnification shows a very thin carbonaceous layer (Fig. 13L), which lies next to the far thicker silicon, and magnesium enrichment layer. At this magnification, a relative aluminum enrichment is now also visible coincident with the silicon and magnesium layer (Fig. 13K shows the aluminum layer). A close inspection of Fig. 13A shows that the translucent brown layer of the carbonaceous compression in the black boxed section corresponds most closely to the magnesium, aluminum, and silicon enrichments seen in Fig. 13E-F and K. This chemical suite of enrichments, along with the translucent layer's pleochroism suggests that the layer consists of aluminosilicate clay or its derivative.

Small Chuaria *from the Sifangtan and Jiulongwan sections*

Analyses of the small *Chuaria* found throughout Member II of the Doushantuo Formation at the Sifangtan Section and in the upper Member II of the Doushantuo Formation at the Jiulongwan section revealed surprising results when compared to the *Chuaria* of the Sixi and lower Member II Jiulongwan sections. The lithology containing the small *Chuaria* fossils is an argillaceous dolostone, similar to the fossiliferous Sixi section. Compared to the Sixi and lower Member II Jiulongwan *Chuaria* fossils, the small *Chuaria* fossils at Sifangtan and the upper Member II Jiulongwan are noticeably smaller, fainter, and more densely clustered (Fig. 14A-C).

Plane view elemental analyses of two small *Chuaria* specimens (SFT-24-1-#6 and #7) reveal very different elemental distributions from the *Chuaria* fossils of the Sixi and Jiulongwan sections (Fig. 14E-I). The fossils have a conspicuous elevation of carbon relative to the background (Fig. 14E) and a relative depletion of silicon (Fig. 14F). Iron has only points of

relative enrichment within the fossils (Fig. 14H). Magnesium enrichment is even throughout the sample (Fig. 14G), and point analyses of the matrix show magnesium mass percentages to be somewhat lower than that of calcium (11% to 15%), which is near the approximate 3:5 weight percent ratio expected for a dolomitic matrix.

Analysis of a small *Chuaria* fossil in cross section (SFT-15-2-#9) revealed more on the nature of iron enrichment in the fossil. A view of the fossil in plane polarized light (Fig. 15A) shows the carbonaceous compression, which was found in a layer bearing abundant small *Chuaria* fossils, preserved as a lens of dense opaque material. This opaque material is framboidal, as shown in BSE images (Fig. 15B-C). Elemental analysis shows that while most of the framboids contain iron oxide (Fig. 15D-G), some towards the center of the structure are pyritic (Fig. 15F-G). Carbon enrichment is not present in the carbonaceous compression (Fig. 15H). Most likely, pyrite framboids were originally present in the carbonaceous compression, but were subsequently weathered to iron oxides. Any organic carbon, if originally present, must also have been weathered, or may simply be hidden underneath the great cluster of framboids. Given the predominance of pyrite framboids and their weathered products in this fossil, the discrete iron-enriched points in the small *Chuaria* specimen illustrated in Fig. 14A and D-I may also represent residual pyrite framboids.

Vendotaenia *fossils from the Miaohe and Huajipo sections*

The *Vendotaenia* fossils for this study occur solely within the siltstone laminae of the Shibantan Member of the Denying Formation, sandwiched between layers of recrystalized bituminous limestones. Weathering is a more prominent issue with this lithology than it is for those bearing *Chuaria* fossils. The fresh siltstone is very dark, nearly black, and *Vendotaenia*

fossils can be seen as thin silvery films on the bedding planes of the siltstone (Fig. 16A). However, fresh siltstone was hard to find. The one fresh piece came from a newly blasted section at the Wuhe locality. Usually, the siltstone beds are weathered to a buff color. This resulted in *Vendotaenia* specimens that are more easily recognizable (Fig. 16B) but more difficult to analyze.

A moderately weathered specimen from the Miaohe section was the first selected for analysis (MH-7-#1; Fig. 17A). The carbonaceous compression itself came from a bedding plane that opened up as the sample was prepared, and consists of several intertwined *Vendotaenia* ribbons with an ellipsoidal stain in the middle. Elemental mapping of an area where a ribbon and the stain intersect shows the ribbons to be barely enriched in aluminum, carbon, and iron (Fig. 17C, F, and I), with a strong enrichment in calcium and sulfur (Fig. 17G-H). Although some carbon is detectable on the *Vendotaenia* specimen (Fig. 17F) point analysis shows that carbon forms a relatively small mass percentage of the material in the fossil: 11% in the ribbon and 6% in the stain (Table 1). However, point analysis shows that oxygen represents 40% of the mass in the ribbon and 38% of the mass in the stain. This, along with the strong relative enrichments of calcium and sulfur, suggests that the compressions are primarily made of calcium sulfate, either gypsum or anhydrite. This is most likely a weathering product of pyrite.

A cross-section from the aforementioned newly blasted specimen (SBT-9) was also made, and many *Vendotaenia* fossils could be seen in cross-section on a bedding plane that was partially exposed and contained abundant *Vendotaenia* specimens in plane view (Fig. 16A). Unlike the *Chuaria* from the Sixi and Jiulongwan sections, it can be seen that the carbonaceous compression is not only very thin, but is also opaque in transmitted light (Fig. 16C). As such it shows neither pleochroism nor extinction. One of these fossils in cross section was analyzed and

elementally mapped (SBT-9-#3), and an image of it in BSE mode is characterized by a low elemental weight when compared to the matrix (Fig. 18A). While the fossil itself has an almost gummy texture, the matrix is clearly made of recrystallized calcite rhombs (Fig. 18B). Elemental mapping shows a depletion in oxygen and calcium (Fig. 18C, E) and an intense enrichment of carbon and sulfur (Fig. 18F-G) in the area of the *Vendotaenia* fossil. There is a separation between the areas of enrichment in carbon and sulfur in the *Vendotaenia* fossil similar to the separation between the carbon-rich layer and aluminum-magnesium-silicon-rich layer in the *Chuaria* fossils. Unlike in the *Chuaria* cross-sections, this separation was not mutually exclusive. Point analysis shows that there is a strong presence of oxygen in the carbonaceous compression of about 22 to 25% (wt); this is about twice the amount of sulfur, which ranges from 13 to 14% (wt) (Table 1). Since sulfur has twice the mass of oxygen, these are the expected elemental abundances for sulfate minerals (SO_4^{2-}), but there are not enough cations present to balance the sulfate (calcium is present only at 4% by mass in the compression). Since sulfate does not bond to reduced carbon readily, the exact chemical and mineralogical composition of the *Vendotaenia* ribbon cannot be determined at this point.

Raman spectroscopy results

Raman analysis of specimens from both the Doushantuo and Denying formations show that the rocks are rich in organic carbon. Simply pointing at the matrix is sufficient to find a strong raman shift for organic carbon. *Chuaria* specimens from the argillaceous dolostone and calcareous siltstone lithologies from the Sixi section, *Chuaria*, *Tawuia*, and bacterial mat specimens from the calcareous siltstone facies from the lower Jiulongwan section, and small *Chuaria* specimens from the Sifangtan locality were selected for further study. The results are presented in Table 1. The D:G ratio presented in the final column is a measurement of the

relative thermal maturity of the sample. The D:G ratio is a rough estimate of the amount of aliphatically bonded and otherwise "disordered" carbon (the D band) compared to doubly bonded carbon-carbon bonds, as in aromatic cycles (the G band). As kerogens mature, their G band becomes more intense as the D band lowers in intensity; thus, a lower D:G ratio indicates a more thermally mature organic carbon. Figure 19D shows that most of the specimens analyzed had relatively comparable D:G ratios in the range of 0.45 to 0.55. Only the small *Chuaria* specimens from the Sifangtan section had a considerably higher D:G ratio (near 0.65; Fig. 19A) than the other analyzed specimens, indicating that the small *Chuaria* fossils here are relatively less thermally mature than the *Chuaria*, *Tawuia*, and bacterial mat specimens from the Sixi and Jiulongwan sections.

Population analysis of Chuaria

Analyses examining the spatial dimensions of *Chuaria* (Table 2) from the argillaceous dolostone at the Sixi section (n=24), calcareous siltstone at the lower Jiulongwan section (n=55), and small *Chuaria* fossils from the Sifangtan and upper Member II Jiulongwan sections (n=92) support that there is more than one population of *Chuaria* present in the Doushantuo Formation. Log transformed axis measurements were used to calculate a log transformed surface area that was then used for statistical analysis. Operating under the null hypothesis that the three samples of *Chuaria* should come from the same population, one-way ANOVA of the three samples shows statistically significant evidence to reject this hypothesis (Table 3). Examination of the relation of the sample means to the grand means (Fig. 20A) suggests that it is the small *Chuaria* fossils that generate the statistically significant result. Further ANOVA tests confirm this: when only the Sixi section argillaceous dolostones and lower Jiulongwan section calcareous siltstones

are statistically tested, the null hypothesis cannot be rejected (p=0.66; Fig. 20B). Lumping *Chuaria* fossils from the Sixi section and lower Member II at Jiulongwan section as a single sample and testing this combined sample against the small *Chuaria* fossils returns an even larger F-value than when all three samples are tested separately (Table 3; Fig. 20C).

DISCUSSION

Trends in Observations of Carbonaceous Compressions

The current taphonomic understanding of carbonaceous compressions emphasizes the need to halt the degradation of nonbiomineralized remains. Organic degradation comes in three varieties: autolytic decay, aerobic decay, and anaerobic decay. Just how all three processes can be stopped has been debated by many authors, and different authors have mainly emphasized the importance of single factors for the preservation of carbonaceous compression fossils (Allison, 1988; Butterfield, 1990; Aronson, 1992; Allison, 1993; Butterfield, 1995; Orr, 1998; Briggs, 2003; Butterfield, 2003; Orr, 2003; Gabbot, 2004; Gaines, 2005; Butterfield, 2007; Gaines, 2008; Page, 2008). A summary of the various factors that might affect organic degradation and their relationship to one another is presented in Fig. 21.

Some speculative hypotheses have become apparent in the recent taphonomic study of carbonaceous compressions. First is that there are many important factors that control the preservation of organic remains, and a number of conditions must be satisfied for this style of preservation to occur. Second, there may be multiple ways these factors can come together to allow for the preservation of organic remains. Third, carbonaceous compressions may be preserved in conjunction with other taphonomic pathways described by Butterfield (2003) and discussed by Allison (1998) and Briggs (2003). What follows are some observations which offer support to these three hypotheses. These observations, in turn, allow for the presentation of a more refined taphonomic picture of carbonaceous compressions, and some commentary on why

the taphonomic path was so prevalent and of such high preservational quality in the Neoproterozoic and Cambrian.

First to contend with are those observations which support the three hypotheses, but differ from current understandings. It has long been held that carbonaceous compressions can only be preserved in calm, still waters with a minimum of bioturbation (Orr, 2003; Gaines, 2005; Brett, 2009). The presence of numerous and well-preserved *Chuaria* fossils in association with dolomitic packstones (Figs. 3A, 12A and C), some with evidence of local winnowing (Fig. 3B) offers contrary evidence to this assertion. The presence of thin lag deposits of phosphatic grains (Fig. 3B) along with the presence of scours, laminites, graded beds, and breccia beds present in other sections of the Doushantuo Formation with a similar lithology (McFadden, 2009) suggests some wave or current activities. While it is true that *Chuaria* is among the most robust of the organic-walled microfossils and could be preserved in conditions that would destroy more fragile carbonaceous compressions, the fact remains that there are abundant *Chuaria* fossils in what may be interpreted as shallow water packstones. While calm, relatively deep waters may be a necessity for exceptional carbonaceous compressions, the taphonomic pathway itself need not be restricted to these environments.

This study also offers new insights into the microchemical distribution of elements in carbonaceous compressions. Orr et al. (2009) proposed two end member configurations as to how clay coats are physically associated with carbonaceous material in a carbonaceous compression. Either the organic carbon may be surrounded by clay, or the clay may be surrounded by carbon. As shown in Fig. 13K-L, though, clay coats can be strongly concentrated to one side of the carbonaceous compression, and do not need to be "sandwiched" between two organic layers. Such a configuration would help to explain why there is a paucity of carbon in

the weathered *Tawuia* specimen of Fig. 11 and an enrichment of carbon in the weathered *Chuaria* specimen of Fig. 10: the "missing" elements (carbon and clay coat elements like aluminum, magnesium, and silicon in the case of the *Tawuia* specimen; and aluminum, magnesium, and silicon in the case of the weathered *Chuaria* specimen) could be present on the counterparts of the analyzed specimens. The presence of clay coats on only one side of a carbonaceous compression does raise the question of how this configuration formed. Furthermore, the clay coat forms a layer that is far thicker than that of the kerogenized organic carbon. Since it has been hypothesized that the growth of clay minerals on carbonaceous compressions is primarily a consequence of diagenesis (Butterfield, 2007; Gaines, 2008), it is possible that as the organic carbon underwent diagenesis, the mass loss associated with organic maturation opened up space for the precipitation of clays. The factors that determine whether the clays would have formed in the configurations outlined by Orr et al. (2009) or in the manner seen in this study cannot yet be determined. Testing to see if clay configurations correspond to specific sediment types or taxonomic groups, or if one-sided clay coats consistently form above or below the organic carbon layers would be some first steps to take to investigate this issue.

The current hypothesis that clay coats on carbonaceous compression tend to become thicker and more extensive with an increasing degree of diagenesis or metamorphism (Gaines, 2005; Butterfield, 2007; Page, 2008) is supported in this study. Specifically, Raman analysis shows the small *Chuaria* fossils of the Sifangtan section to have a higher D:G ratio than the *Chuaria* fossils typical of the Jiulongwan and Sixi sections (Table 1; Fig. 19A-B). This indicates that the small *Chuaria* specimens are less thermally mature than their larger counterparts from elsewhere in the Doushantuo Formation. As the hypothesis predicts, while small *Chuaria* specimens show virtually no aluminosilicate element enrichment around the area of the fossils

(Fig. 14F-G), *Churia* specimens from Sixi and lower Member II at Jiulongwan have a robust aluminum-magnesium-silicon clay coat (Fig. 13D-F and L). This coat is thick enough to all but obscure the carbon of the carbonaceous compression in plane view (Fig. 6H, 7F, 9G). This preservational difference could be due to more than just different degrees of diagenetic alteration, however. Since the small *Chuaria* fossils from the Sifangtan can be considered to be of a separate population than those of the Sixi and lower Member II at Jiulongwan sections (Fig. 20C), it is possible that the small *Chuaria* specimens had a different organic-wall composition in life. The small *Chuaria* specimens would then be preserved as carbonaceous compressions with a distinct organic carbon composition independent from thermal maturity. The small *Chuaria* fossils could have an outer wall richer in unordered, aliphatic chain carbons, giving a Raman spectrum that would be equivalent to a less thermally mature *Chuaria* fossil from Sixi or lower Member II at Jiulongwan. It is unlikely that all of the difference in the D:G ratio could be explained through differences in the fossils' outer wall, though. The lack of clay coats around the small *Chuaria* supports that at least some of the D:G ratio difference is due to different diagenetic histories.

This study can also offer an explanation as to why Gabbot et al. (2004) were unable to find organic carbon enrichment associated with their Maotianshan carbonaceous compressions. This study has shown that the presence of sulfur and pyrite in conjunction with carbonaceous compressions is not unusual. Pyrite framboids were seen associated with many *Chuaria* specimens (Fig. 9B and H-I, 10B and H-I, 14H) and sulfur is also present in intimate association with *Vendotaenia* specimens (Fig. 17H, 18G). The presence of pyrite indicates the inception of sulfate reduction by anaerobic bacteria, which degrade organic remains. In cases where sulfate reduction is allowed to continue, the situation illustrated in Fig. 15 may result. The small

Chuaria specimen has been thoroughly degraded by sulfate reducers and nearly completely casted by pyrite framboids (some of which have since been altered to iron oxides). Any trace of organic carbon left in the fossil has been obscured by the overwhelming presence of the framboids. These small *Chuaria* fossils and similarly pryitized chuarids from the Lantian Formation (Yuan, 2001) can be taken as end-member examples of what can happen to organic remains if sufficient sulfate is present to support extensive bacterial sulfate reduction. What is more difficult to explain is the presence of sulfur in *Vendotaenia* ribbons (Fig. 18G). There are no readily discernable framboid structures within or on the ribbons, and point analysis does not detect any appreciable amount of iron. The enrichment of sulfur by sulfate reducing bacteria in the ribbons seems possible, but this hypothesis remains unproven until direct evidence of pyrite is found.

A model for the temporal distribution of carbonaceous compressions

One of the most vexing problems of carbonaceous compressions is its temporal distribution. Most of the factors that have a deleterious effect on the preservation of carbonaceous compressions, such as bioturbation or the presence of oxygen in marine sediments (Fig. 21), increased in significance as the Phanerozoic progressed, but such secular changes cannot explain the preferential Neoproterozoic to middle Cambrian distribution of exceptional carbonaceous compression deposits (Butterfield, 1995). If anything, the frequency and quality of exceptional carbonaceous compression deposits should increase further back into the Proterozoic, but this is not seen. Other exceptional preservation taphonomic pathways, most specifically phosphatization and pyritization, showed a similar increase in abundance and fidelity in the Neoproterozoic, followed by a drop after the Cambrian and Ordovician (Butterfield, 2003;

Donoghue et al., 2006). The presence of both phosphatization and pyritization in the Doushantuo carbonaceous compressions analyzed in this study is probably not a coincidence. Here a revised scheme for the preservation of carbonaceous compressions is presented, relating the fidelity of the compressions to the redox state of the basin.

Sulfate reduction and the amount of anaerobic decay is hypothesized to be the key determining factor in whether or not carbonaceous remains can be formed and preserved as carbonaceous compressions. If an unlimited amount of sulfate were available, sulfate reduction would proceed to completely degrade organic matter. Yet with too low a sulfate concentration, geochemical conditions for initial mineralization (via pyrite, phosphate, and clay minerals) and deactivation of autolysis would not be met. With the right amount of sulfate and ferrous iron, pH decline associated with bacterial sulfate reduction and pyrite precipitation would tip the isoelectric balance of autolytic molecules and highly reactive clays, allowing the latter to deactivate the former (Butterfield, 1990). With limited sulfate availability, the precipitation of small amounts of pyrite also provides mechanical protection for the organic remains against complete degradation. In addition, sulfate reduction bacteria can also release phosphate from the decaying organism which, given locally low pH, allows the available calcium to bond with phosphate rather than carbonate and replace the more labile tissues or intracellular material present in the decaying organism (Butterfield, 2003). Extensive pyritization, as in the Ordovician Beecher's Trilobite Bed (Farrel, 2009), probably requires greater sulfate availability and more extensive sulfate reduction of more recalcitrant soft-body parts, such as trilobite limbs. In contrast, the preservation of carbonaceous compressions requires moderate amounts of sulfate reduction to allow for the deactivation of autolytic enzymes.

These conditions require some—but not too much—sulfate and moderately anoxic conditions to allow anaerobic respiration, initial authigenic mineralization, and autolysis deactivation to proceed. This speculation is consistent with geochemical evidence that shows Neoproterozoic to early Cambrian oceans were characterized by ferruginous and sometimes euxinic environments (Canfield and Farquhar, 2009). The Yangtze platform, in particular, was an often anoxic basin during the deposition of the Doushantuo formation (McFadden et al., 2008; Ader et al., 2009; Li et al., 2010). The Yangtze Gorges area is interpreted as a partly restricted intracratonic basin where baisnwide conditions of anoxia could easily develop and create conditions that promoted carbonaceous compressions and other modes of exceptional preservation (e. g. silicification, pyritization). These ideal conditions could often emerge during the Cambrian as well, where the evolution of more recalcitrant cuticles allowed for carbonaceous compressions to preserve incredible amounts of anatomical detail. As the Phanerozoic progressed, however, increasing amounts of sulfate in the water column, more deeply oxygenated waters, and more intensive bioturbation (Aronson, 1992; Aronson, 1993; Orr et al., 2003; Canfield and Farquhar, 2009) made exceptional carbonaceous compressions increasingly difficult to form and preserve in the marine realm. While carbonaceous compressions could still be found, of course, such as in the preserved periderm of graptolites or leaves, the fidelity of the Neoproterozoic and Cambrian carbonaceous compressions in marine environments was all but extinguished.

CONCLUSIONS

Carbonaceous compressions are too common in the fossil record and hold too many unique glimpses into the history of life not to be thoroughly understood on a taphonomic level. Elemental analysis of *Chuaria* and *Vendotaenia* from the Doushantuo and Denying formations in the Yangtze Gorges area offers many clues to this preservational pathway, and this study has shown the taphonomy of carbonaceous compressions to be even more complex than previously thought. It may be that carbonaceous compressions are every bit as variable as more common preservational pathways, such as calcification. If this is true, much work needs to be done to understand the ultrastructure and microchemistry of a range of carbonaceous compressions before we can begin to arrive at some general conclusions about the taphonomic conditions and processes responsible for the preservation of carbonaceous compressions. This study is a first attempt in this direction. Further work should concentrate on how carbonaceous compressions are related with other exceptional preservation pathways, such as phosphatization and pyritization. Other areas for study include the variety and abundance of various clay coats on organic substrates, and how pyrite could serve to affect the fidelity of carbonaceous compressions. While *Chuaria* and *Vendotaenia* are great candidates for this further research, other carbonaceous compressions should also be examined to test the general applicability of the conclusions reached in this study to the taphonomy of carbonaceous compressions as a whole. In particular, exploration of earlier Proterozoic carbonaceous compressions like acritarchs could generate interesting results.

REFERENCES

ADER, M., MACOUIN, M., TRINDADE, R. I. F., HADRIEN, M-H., YANG, Z., SUN, Z., AND BESSE, J., 2009, A multilayered water column in the Ediacaran Yangtze platform? Insights from carbonate and organic matter paired ∂13C: Earth and Planetary Science Letters, v. 288, p. 213-227, doi: 10.1016/j.epsi.2009.09.024.

ALLISON, P.A., 1988, *Konservat-Lagerstäten:* cause and classification: Paleobiology, v. 14, p. 331-334.

ALLISON, P.A., & BRIGGS, D. E. K., 1993, Burgess Shale biotas: burrowed away?: Lethaia, v. 26, p. 184-185.

ARONSON, R.B., 1992, Decline of the Burgess Shale fauna: ecologic or taphonomic restriction?: Lethaia, v. 25, p. 225-229.

ARONSON, R.B., 1993, Burgess Shale-type biotas were not just burrowed away: reply: Lethatia, v. 26, p. 185.

BRETT, C.E.A., P. A.; DESANTIS, M. K.; LIDDELL, W. D.; & KRAMER, A., 2009, Sequence stratigraphy, cyclic facies, and *lagerstatten* in the Middle Cambrian Wheeler and Marjum Formations, Great Basin, Utah: Palaeogeography, Palaeoclimatiology, Palaeoecology, v. 277, p. 9-33.

BRIGGS, D.E.G., 2003, The Role of decay and mineralization in the preservation of soft-bodied fossils: Annu. Rev. Earth Planet. Sci., v. 31, p. 275-301, doi: 10.1146/annurev.earth.31.100901.144746.

BRIGGS, D.E.G., ERWIN, D. H., AND COLLIER, F. J., 1994, The Fossils of the Burgess Shale: Smithsonian Institution Press, Washington, 238 p.

BUTTERFIELD, N.J., 1990, Organic preservation of non-mineralizing organisms and the taphonomy of the Burgess Shale: Paleobiology, v. 16, p. 272-286.

BUTTERFIELD, N.J., 1995, Secular distribution of Burgess-Shale-type preservation: Lethaia, v. 28, p. 1-13.

BUTTERFIELD, N.J., 2003, Exeptional Fossil Preservation and the Cambrian Explosion: Integrative and Comparative Biology, v. 43, p. 166-177.

BUTTERFIELD, N.J., BALTHASAR, U., AND WILSON, L. A., 2007, Fossil diagenesis in the Burgess Shale: Palaeontology, v. 50, p. 537-543.

CANFIELD, D.E., AND FARQUHAR, J., 2009, Animal evolution, bioturbation, and the sulfate concentration of the oceans: PNAS, v. 106, p. 8123-8127, doi: 10.1073/pnas.0902037106.

CHIN, K., EBERT, D. A., SCHWEITZER, M. H., RANDO, T. A., SLOBODA, W. J., AND HORNER, J. R., 2003, Remarkable preservation of undigested muscle tissue within a Late Cretaceous tyrannosaurid coprolite from Alberta, Canada: Palaios, v. 18, p. 286-294, doi: 0883-1351/03/0018-0000/$3.00.

DONOGHUE, P.C.J., KOUCHINSKY, A., WALOSZEK, D., BENGSTONE, S., DONG, X., VAL'KOV, A. K., CUNNINGHAM, J. A., AND REPETSKI, J. E., 2006, Fossilized embryos are widespread but the record is temporally and taxonomically biased: Evolution & Development, v. 8, p. 232-238.

FARREL, U.C., MARTIN, M. J., HAGADORN, J. W., WHITELEY, T., AND BRIGGS, D. E. G., 2009, Beyond Beecher's Trilobite Bed: widespread pyritization of soft tissues in the Late Ordovician Taconic foreland basin: Geology, v. 37, p. 907-910, doi: 10.1130/G30177A.1.

GABBOT, S.E., XIAN-GUANG, H., NORRY, M. J., AND SIVETER, D. J., 2004, Preservation of Early Cambrian animals of the Chengjiang biota: Geology, v. 32, p. 901-904, doi: 10.1130/G20640.1.

GAINES, R.R., BRIGGS, D. E. G., AND YUANLONG, Z., 2008, Cambrian Burgess Shale-type deposits share a common mode of fossilization: Geology, v. 36, p. 755-758.

GAINES, R.R., KENNEDY, M. J., AND DROSER, M. L., 2005, A new hypothesis for organic preservation of Burgess Shale taxa in the middle Cambrian Wheeler Formation, House Range, Utah: Palaeogeography, Palaeoclimatiology, Palaeoecology, v. 220, p. 193-205.

HOFFMANN, H.J., AND CHEN, J., 1981, Carbonaceous megafossils from the Precambrian (1800 Ma) near Jixian, northern China: Canadian Journal of Earth Sciences, v. 18, p. 443-447.

HOFMANN, H.J., 1994, Proterozoic carbonaceous compressions ("metaphytes" and "worms"), *in* Bengston, S., ed., Early Life on Earth: Columbia University Press, New York, p. 342-357.

JAVAUX, E.J., MARSHALL, C. P., AND BEKKER, A., 2010, Organic-walled microfossils in 3.2-billion-year-old shallow-marine siliciclastic deposits: Nature, v. 463, p. 934-938, doi: 10.1038/nature08793.

KUMAR, S., 2001, Mesoproterozoic megafossil *Chuaria-Tawuia* association may represent parts of a multicellular plant, Vindhyan Supergroup, Central India: Precambrian Research, v. 106, p. 187-211.

LI, C., LOVE, G. D., LYONS, T. W., FIKE, D. A., SESSIONS, A. L., AND CHU, X., 2010, A stratified redox model for the Ediacaran Ocean: Science, v. 328, p. 80-83, doi: 10.1126/science.1182369.

MCFADDEN, K.A., XIAO, S., ZHOU, C., AND KOWALEWSKI, M., 2008, Quantitative Evaluation of the Biostratigraphic Distribution of Acanthomorphic Acritarchs in the Ediacaran Doushantuo Formation in the Yangtze Gorges area, South China: Virginia Tech., p. 45.

MCFADDEN, K.A., XIAO, S., ZHOU, C., AND KOWALEWSKI, M., 2009, Quantitative Evaluation of the Biostratigraphic Distribution of Acanthomorphic Acritarchs in the Ediacaran Doushantuo Formation in the Yangtze Gorges area, South China: Precambrian Research, v. 173, p. 170-190.

ORR, P.J., BENTON, M. J., AND BRIGGS, D. E. G., 2003, Post-Cambrian closure of the deep-water slope-basin taphonomic window: Geology, v. 31, p. 769-772.

ORR, P.J., BRIGGS, D. E. G., AND KEARNS, S. L., 1998, Cambrian Burgess Shale Animals Replicated in Clay Minerals: Science, v. 281, p. 1173-1175.

ORR, P.J., KEARNS, S. L., AND BRIGGS, D. E. G., 2009, Elemental mapping of exceptionally preserved 'carbonaceous compression" fossils: Palaeogeography, Palaeoclimatiology, Palaeoecology, v. 277, p. 1-8, doi: 10.1016/j.palaeo.2009.02.009.

PAGE, A., GABBOTT, S. E., WILBY, P. R., AND ZALASIEWICZ, J. A., 2008, Ubiquitous Burgess Shale-style "clay templates" in low-grade metamorphic mudrocks: Geology, v. 36, p. 855-858.

SAMUELSSON, J., AND BUTTERFIELD, N. J., 2001, Neoproterozoic fossils from the Franklin Mountains, northwestern Canada: stratigraphic and palaeobiological implications: Precambrian Research, v. 107, p. 235-251, doi: 0301-9268/01/$.

STEINER, M., 1996, *Chuaria circularis* WALCOTT 1899- "megasphaeromorph acritarch" or prokaryotic colony?: Acta Universitatis Carolinae Geologica, v. 40, p. 645-665.

VIDAL, G., 1989, Are late Proterozoic carbonaceous megafossils metaphytic algae or bacteria?: Lethaia, v. 22, p. 375-379.

WANG, X., ERDTMANN, B., XIAOHONG, C., AND XIAODONG, M., 1998, Integrated sequence-, bio- and chemo-stratigraphy of the terminal Proterozoic to Lowermost Cambrian "black rock series" from central South China: Episodes, v. 21, p. 178-189.

XIAO, S., YUAN, X., STEINER, M., AND KNOLL, A. H., 2002, Macroscopic carbonaceous compressions in a terminal Proterozoic shale: a systematic reassessment of the Miaohe Biota, South China: Journal of Paleontology, v. 76, p. 347-376, doi: 0022-3360/02/0076-347$03.00.

YUAN, X., XIAO, S., LI, J., YIN, L., AND CAO, R., 2001, Pyritized chuarids with excystment structures from the late Neoproterozoic Lantian formation in Anhui, South China: Precambrian Research, v. 107, p. 253-263.

ZHANG, X.B., D. E., 2007, The nature and significance of the appendages of *Opabinia* from the Middle cambrian Burgess Shale: Lethaia, v. 40, p. 161-173, doi: 10.1111/j.1502-3931.2007.00013.x.

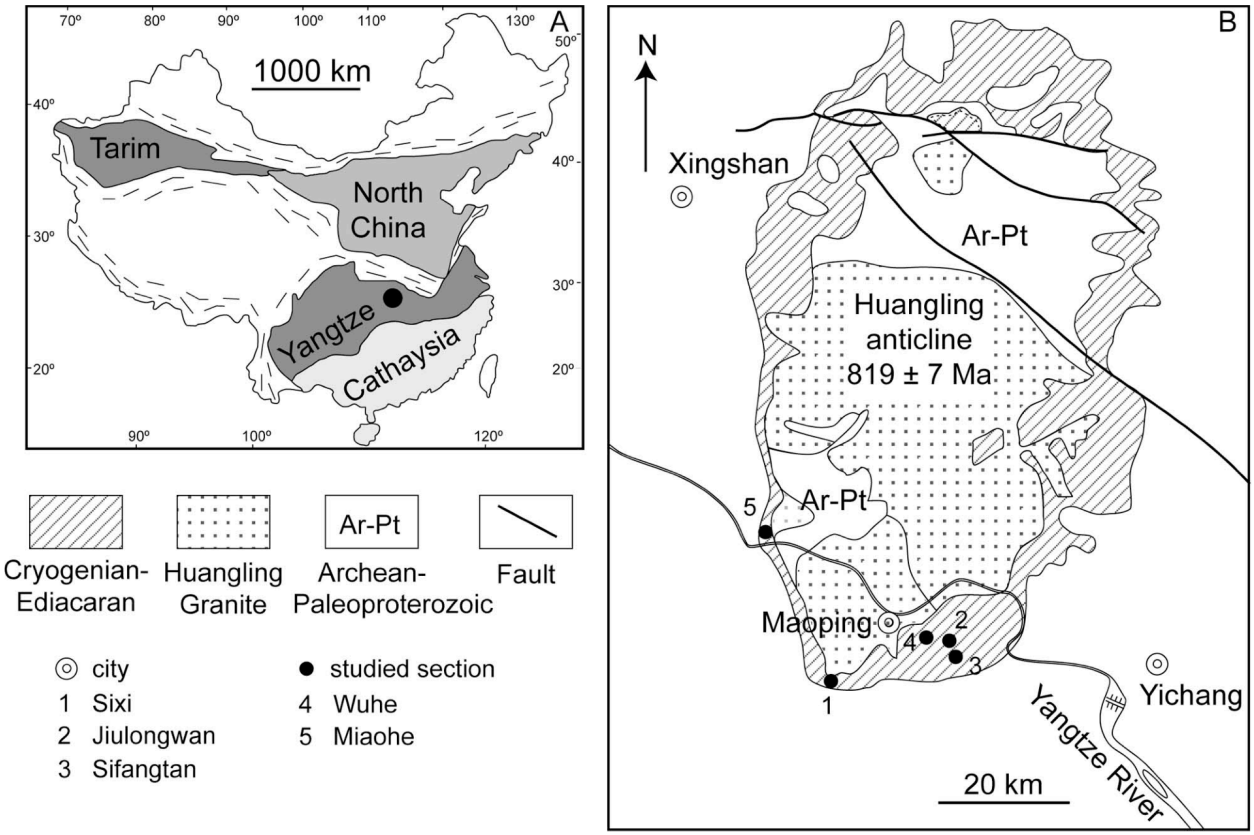

Figure 1- Maps showing the location of the study area on the Yangtze Platform in Hubei Province, China A: Map of China showing the location of the Hunagling Anticline (the black dot, detailed in B) with respect to the major crustal blocks of China. B: Detailed map of the Huangling Anticline, showing the sampling localities.

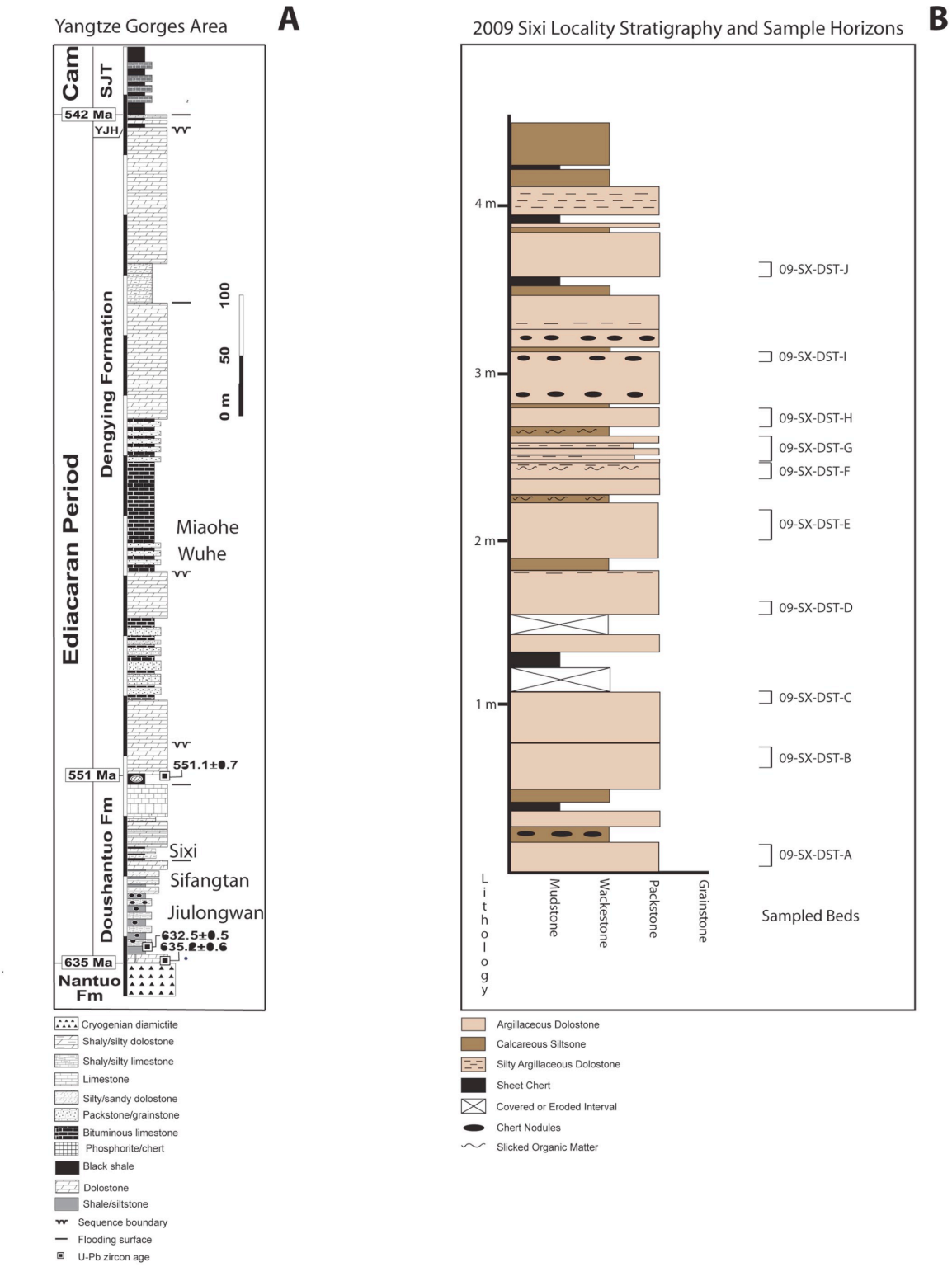

Figure 2: Stratigraphic columns of (A) a generalized column of the Yangtze Gorges area, and (B) the Sixi section showing the stratigraphic horizons where *Chuaria* fossils were collected. In (A), approximate stratigraphic locations of the intervals of the sections used in this study are labeled on the right of the column. Litholoic terms used in (B) correspond to those employed in this study.

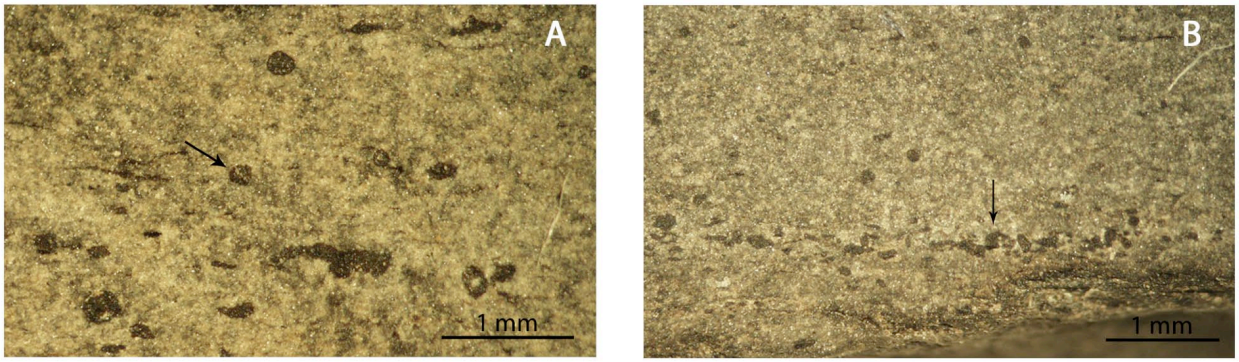

Figure 3- Reflected light photomicrographs of phosphatic grains in polished slabs of argillaceous dolostone cut perpendicular to bedding plane. Samples collected from Sixi Section, sample SX-DST3-3D1c. A: Phosphatic grains (dark color, see arrows) admidst carbonaceous compressions. B: A possible lag deposit of phosphatic grains

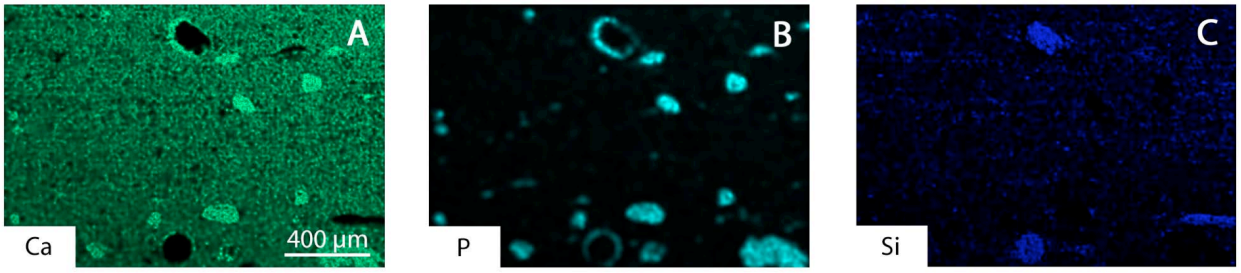

Figure 4- Three elemental maps of sample 08-SX-DST3-3D1e showing phosphatic grains, some of which (at the top and bottom of the images) have a silica core. Scale bar present in (A) applies for (B) and (C) as well.

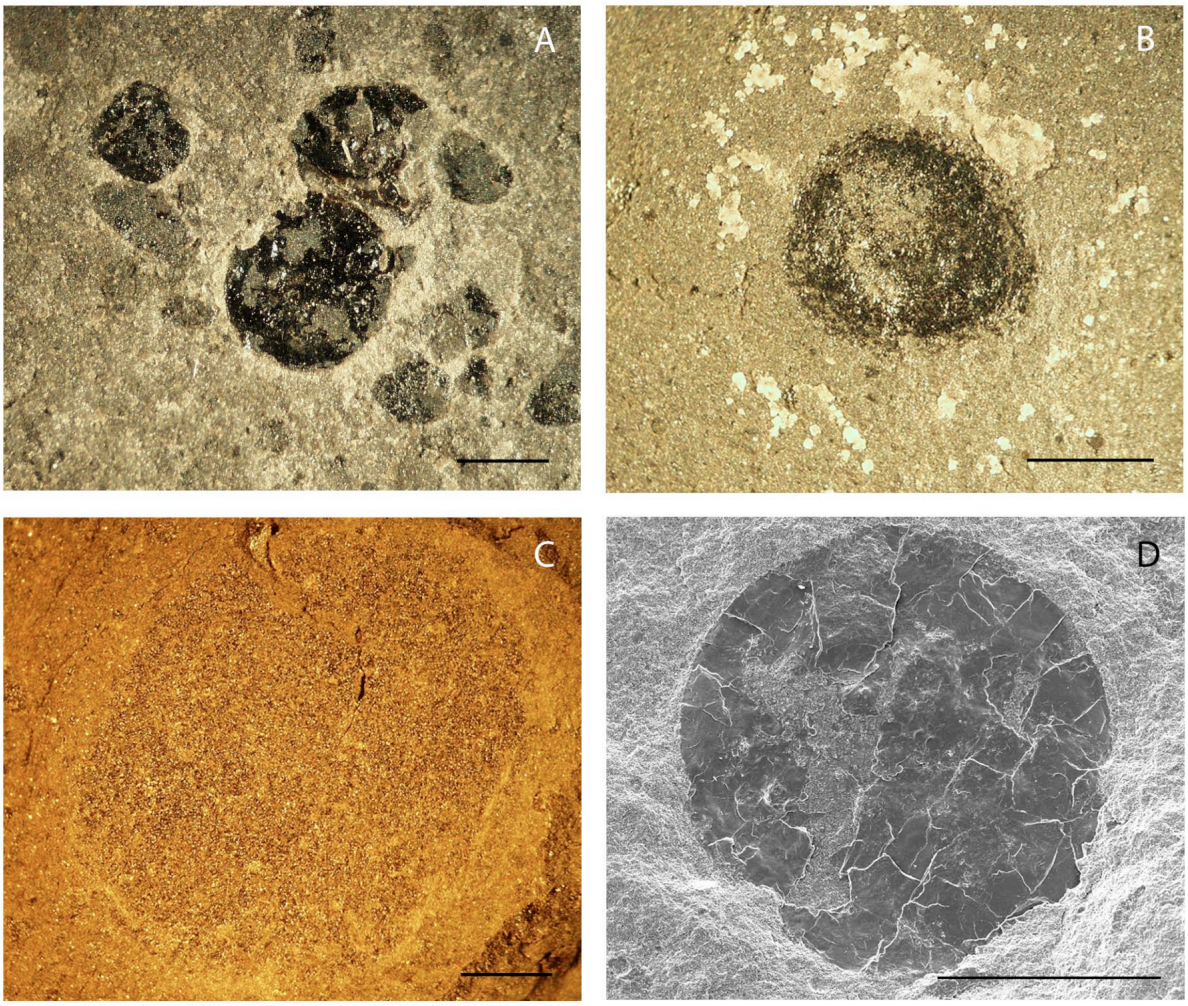

Figure 5- Reflected light photomicrographs (A-C) and BSE imae (D) of *Chuaria* specimens in plane view from the Sixi and Jiulongwan sections. All scale bars are 1 mm long. A:Several *Chuaria* fossils from the Sixi section, specimen numbers 08-SX-DST3-3B1-#5, #6, and #7). B: *Chuaria* from the Jiulongwan Section, specimen number JLW-18B-#1. C: A highly weathered *Chuaria* specimen from the Jiulongwan Section, specimen JLW-18C-#7. D: Back Scattered Electron image of a *Chuaria* specimen from the Sixi section, specimen number 08-SX-DST3-3B3-#5. (All images with fossils in this paper will be labeled according to this format: sample label-#specimen number).

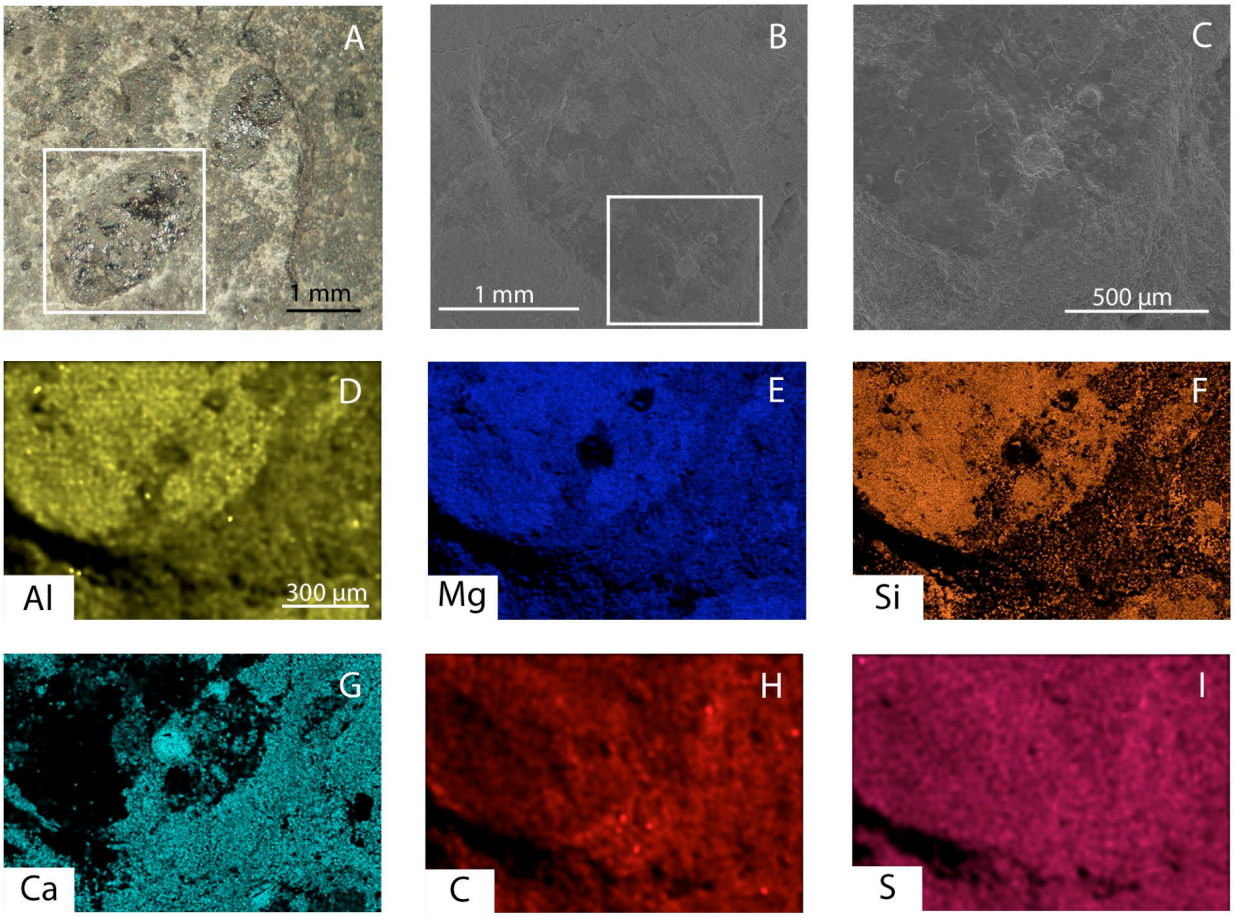

Figure 6- Reflected light photomicrograph (A), BSE image (B-C), and elemental maps (D-I) of a *Chuaria* specimen (08-SX-DST3-3E1b-#1) from Sixi. (B) is a magnified view of marked area in (A). White box in (B) marks area shown in (C-I). Scale bar present in (D) applies to (E-I).

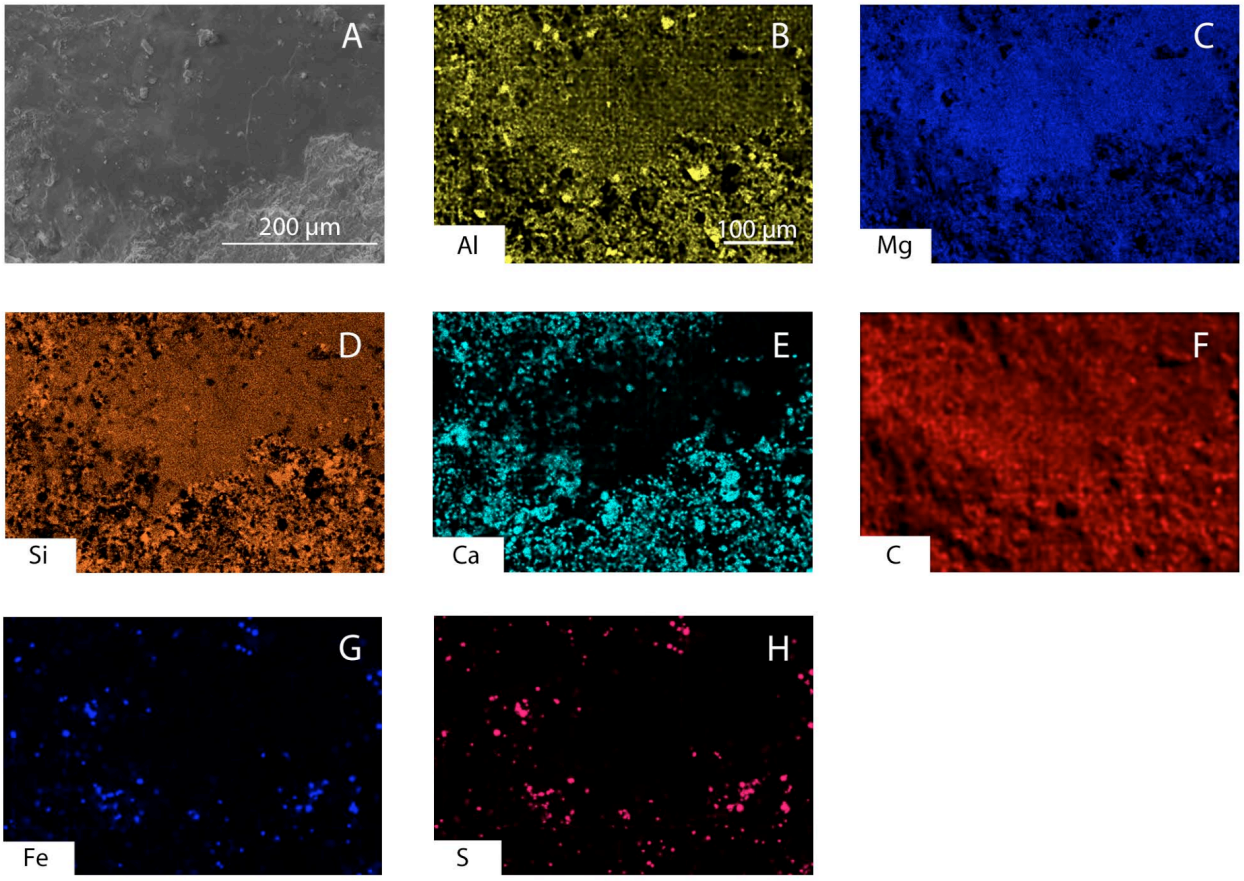

Figure 7- BSE image (A) and elemental maps (B-H) of a probable *Chuaria* fragment (JLW-27Af-#1) from Jiulongwan. Scale bar in (B) applies to (C-H).

Figure 8- Reflected light photomicrograph of two specimens of *Chuaria* (09-SX-DST-F-#1 and #2) from Sixi. The fresh *Chuaria* specimen (#1) is clearly visible on the left side of the chip, and the highly weathered *Chuaria* specimen (#2, about 3mm to the right of #1) just barely so.

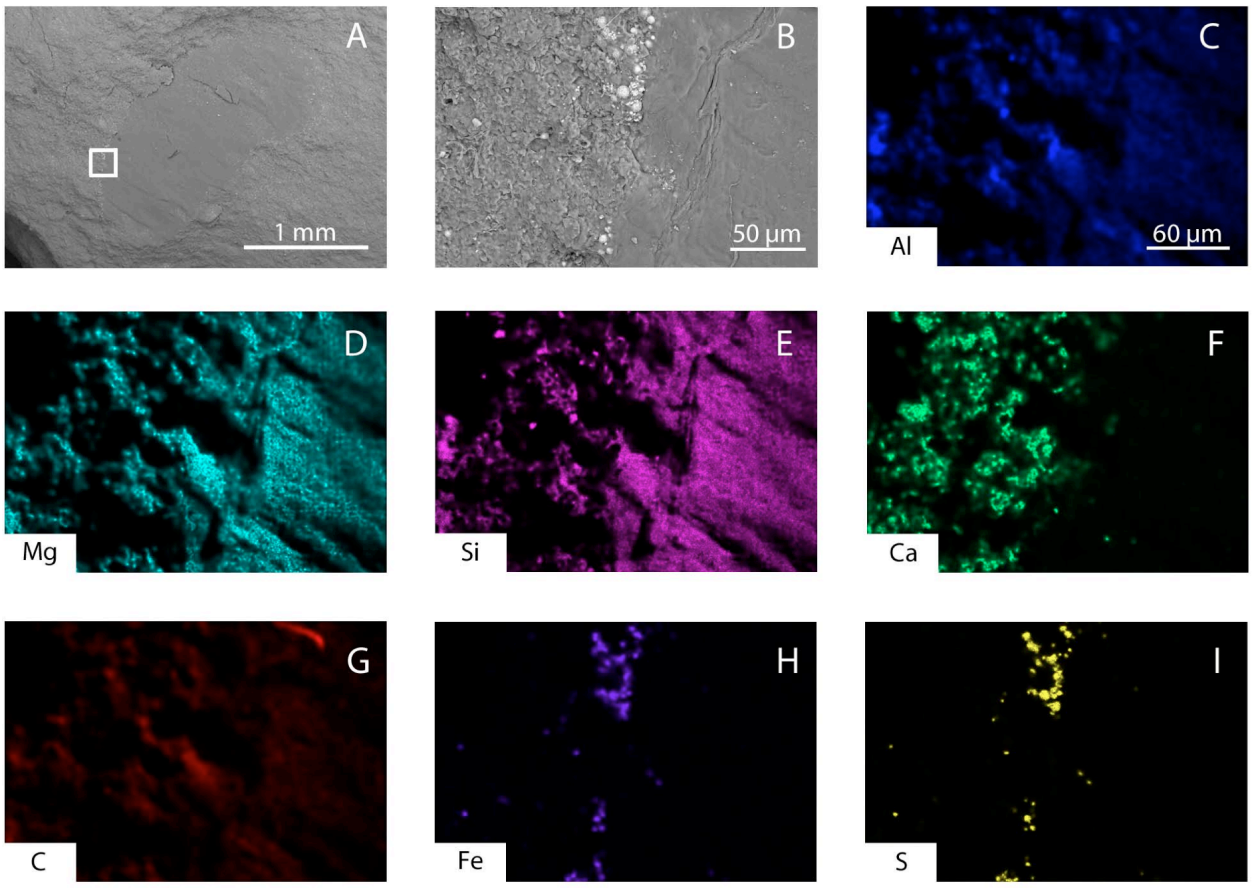

Figure 9- BSE images (A-B) and elemental maps (C-I) of the fresh *Chuaria* specimen illustrated in Fig. 8 (09-SX-DST-F-#1). A: Image of entire *Chuaria*. Note that the fossil appears slightly darker than the matrix. Small white box hightlights the area shown in (B) and elementally mapped in (C-I). B: A close-up of the lower left corner of the fossil. Note the wrinkled texture of the compression and partial halo of framboids. The scale present in (C) applies to (D-I).

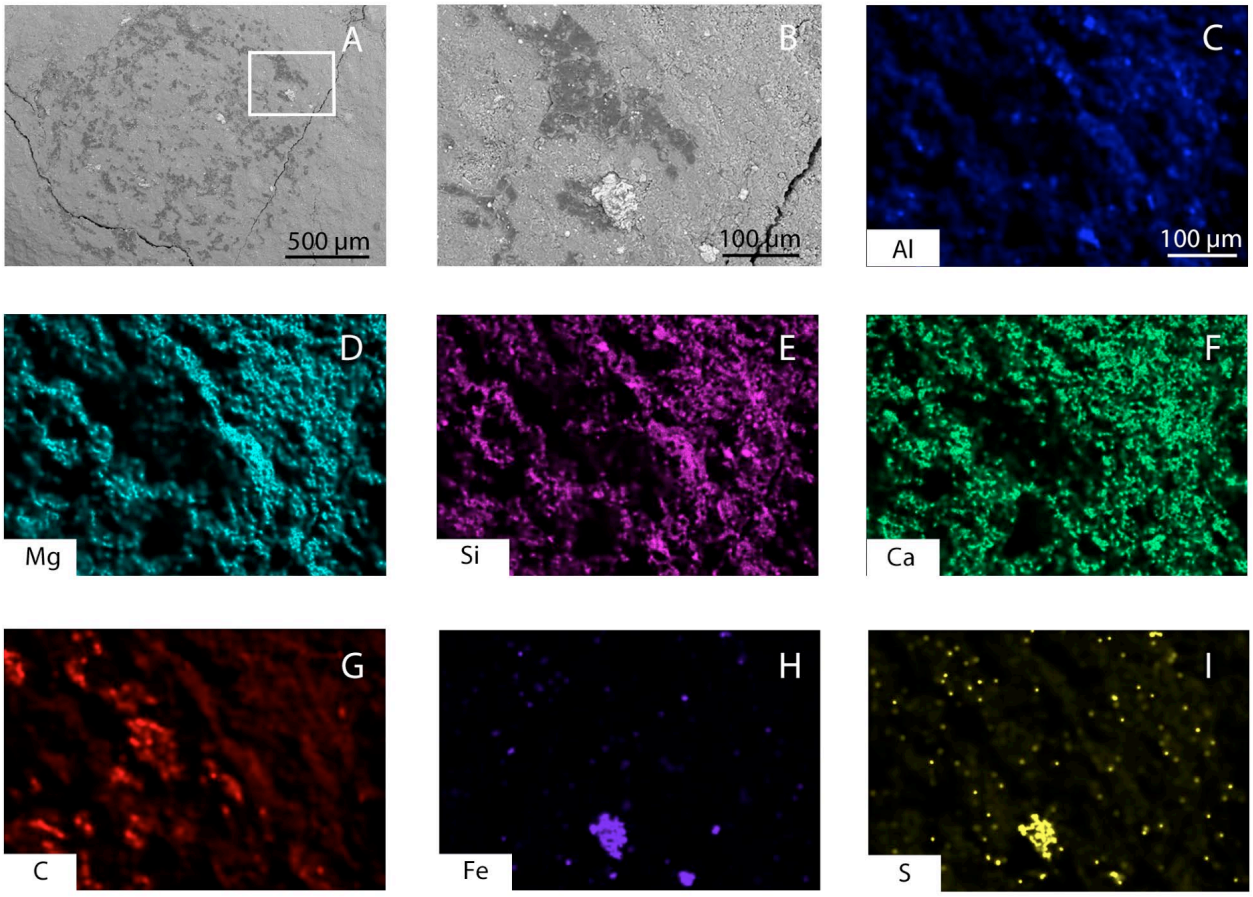

Figure 10- BSE images (A-B) and elemental maps (C-I) of the weathered *Chuaria* specimen illustrated in Fig. 8 (09-SX-DST-F-#2). A: Image of the whole fossil. Note the fragmentary nature of the preservation, and patches of low Z material. The white box indicates the area shown in B and elementally mapped in C-I. B: A close-up of the upper right of the fossil. (C-I) are elemental maps of the area in (B). The scale present in (C) applies to (D-I). Note the framboid clusters visible in the iron and sulfur maps which correspond to the bright patch in (B).

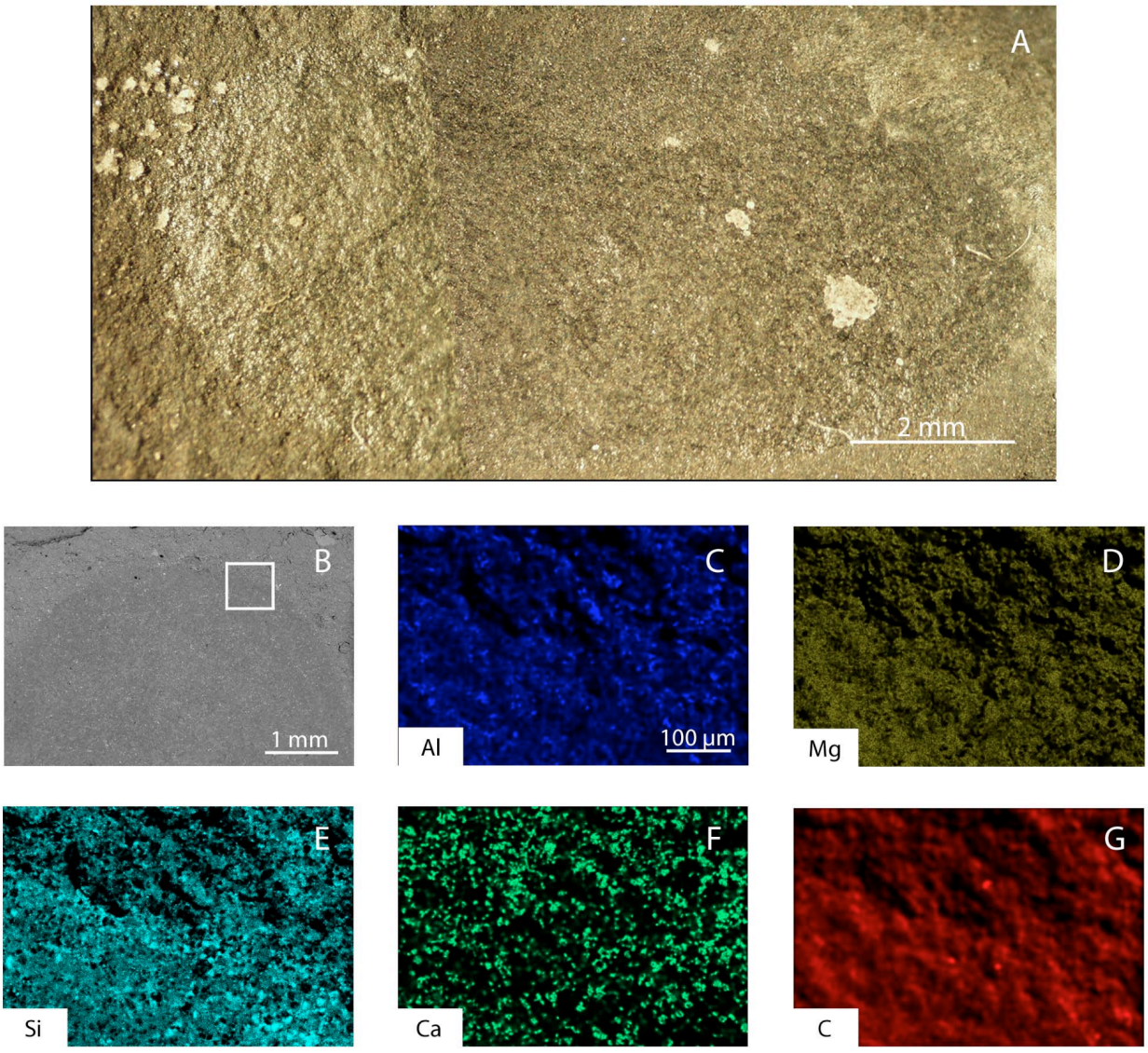

Figure 11- Reflected Light Photomicrograph (A), BSE image (B) and elemental maps (C-G) of a *Twauia* fossil (JLW-18-F-#1) from the calcareous siltstone of the Jiulongwan section. A: Image of the whole fossil. The right end of the *Tawuia* specimen is shown in (B). B: A close-up of the fossil. The white box shows the area analyzed in (C-G). The scale present in (C) applies for (D-G).

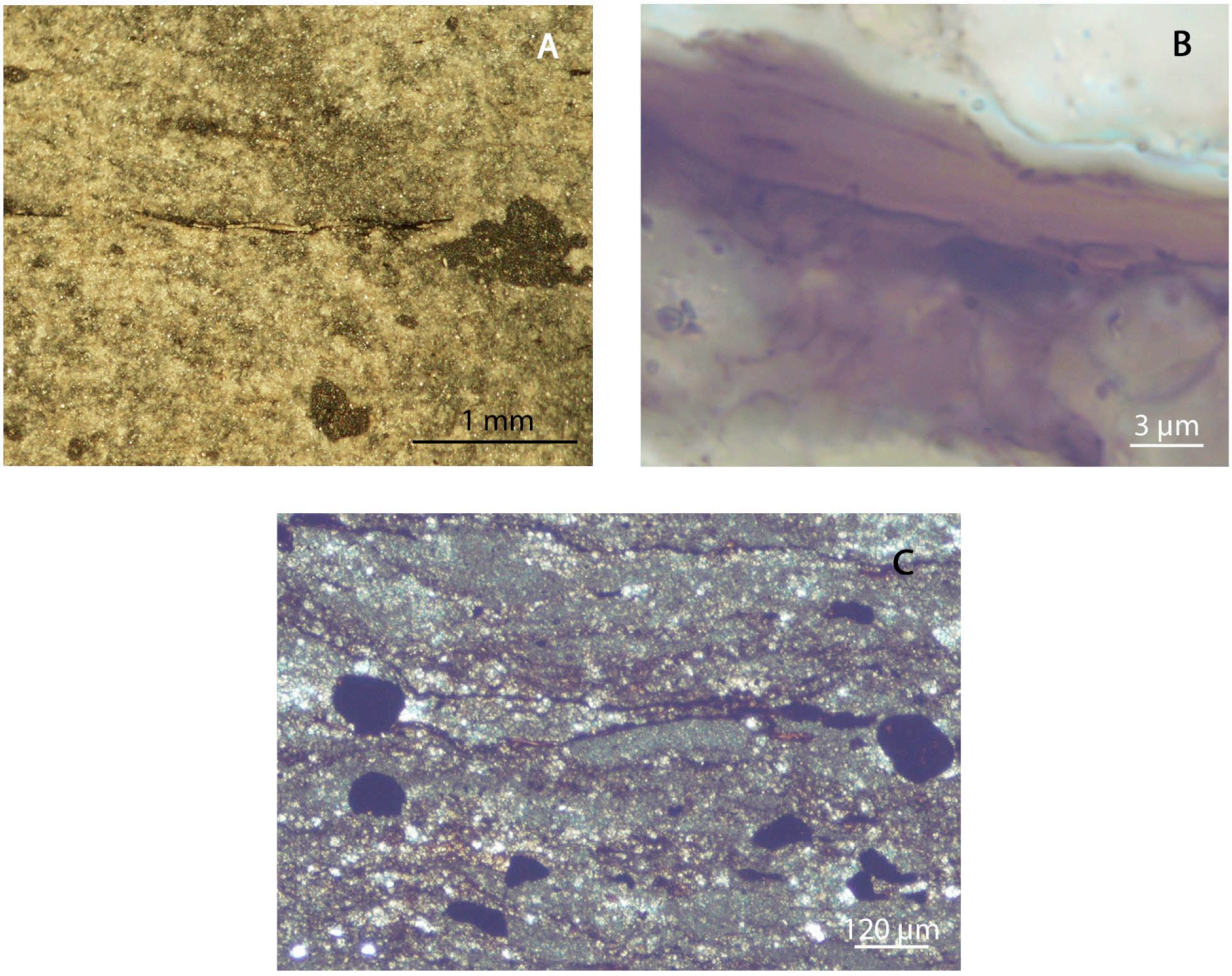

Figure 12- Reflected Light Photomicrograph (A) and Transmitted Light Photomicrographs (B-C) of *Chuaria* specimens in cross section A: A *Chuaria* specimen with a thin internal layer of reflective material (08-SX-DST3-3D1c-#5). B: Segment of a likely *Chuaria* fossil (08-SX-DST3-3A3-#2). C: Portion of a likely *Chuaria* fossil (08-SX-DST3-3A3-#5). The fossil is not totally compressed, but has a lower and upper surface which merge on the right side of the photomicrograph.

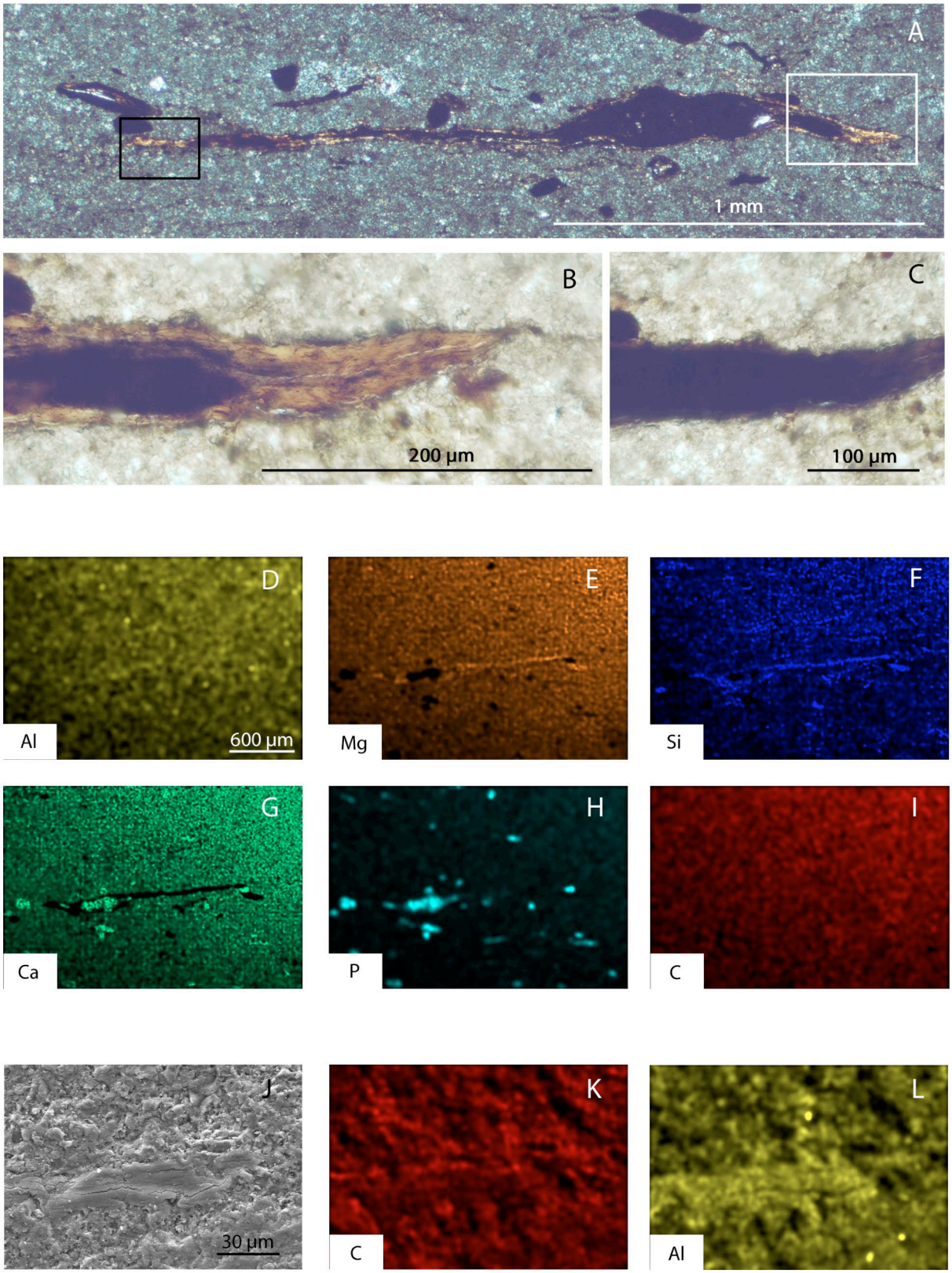

Figure 13- Descriptions of images located on following page.

Figure 13- Transmitted Light Photomicrographs (A-C), BSE image (J), and elemental maps (D-I, K-L) of a large *Chuaria* specimen (08-SX-DST3-3D1e-#1), from Sixi. A: Image of the entire fossil. The white box indicates the area photographed in (B-C). The black box in (A) indicates the area imaged and mapped in (J-L). B: Pleochroic light. C: Pleochroic dark, after 90° rotation. (D-I) are elemental maps of the entire specimen shown in (A). Scale bar present in (D) applies for elemental maps (E-I). Scale in (J) applies for (K-L).

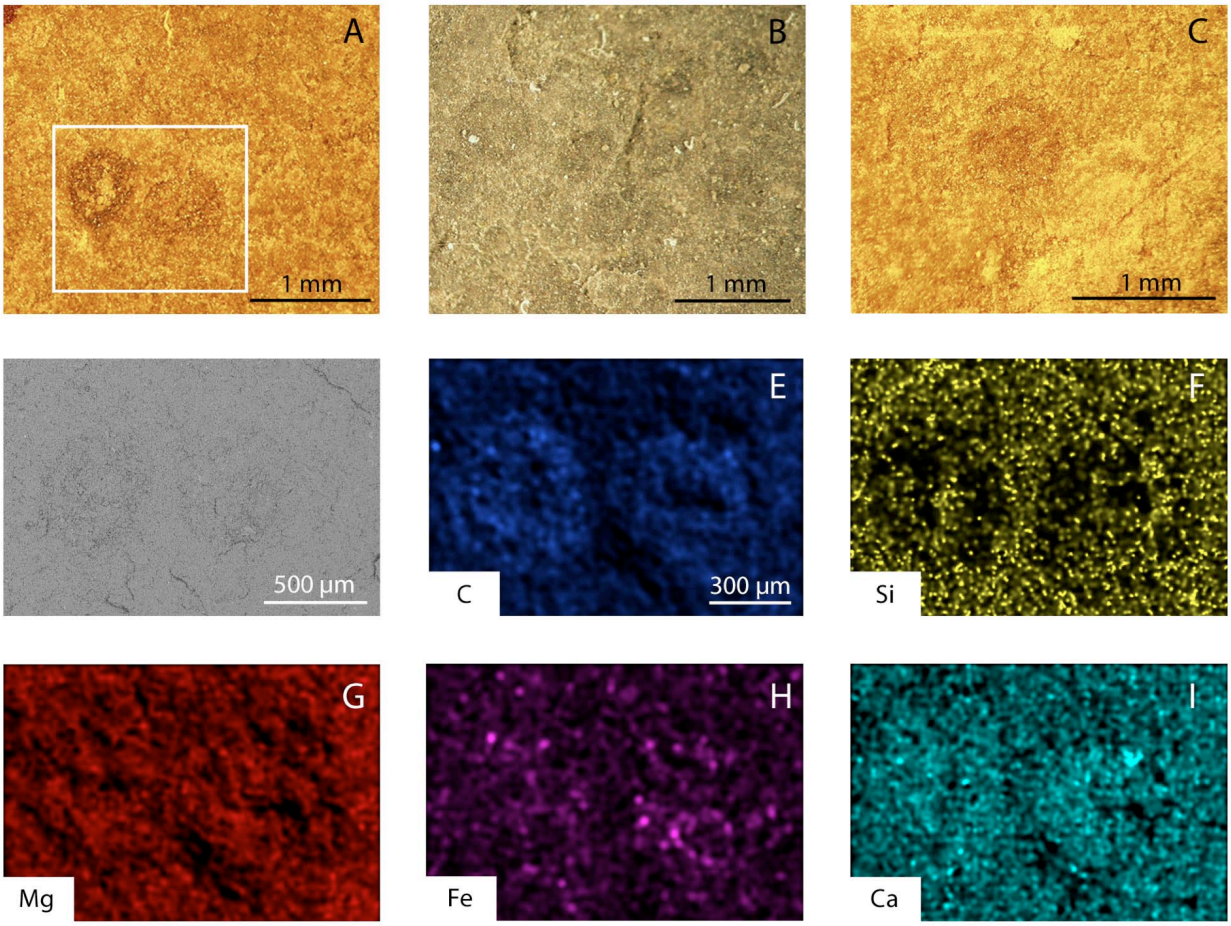

Figure 14- Reflected Light Photomicrographs (A-C), BSE image (D), and elemental maps (E-I) of small *Chuaria* fossils from Sifangtan. A: Pair of small *Chuaria* fossils (SFT-24-1-#6 and 7). White box indicates area imaged in (D) and mapped in (E-I). B: Large cluster of small *Chuaria* fossils (SFT-33.7-#4 and 5). There are at least five whole specimens and many more fragments. However, only two were of sufficiently good quality to be used for analysis. C: Small *Chuaria* specimen with a distinct center (SFT-24-3-#8). D: The two small *Chuaria* specimens seen in (A). (E-I) are elemental maps of the specimens fin (D). Scale present in (E) applies for (F-I).

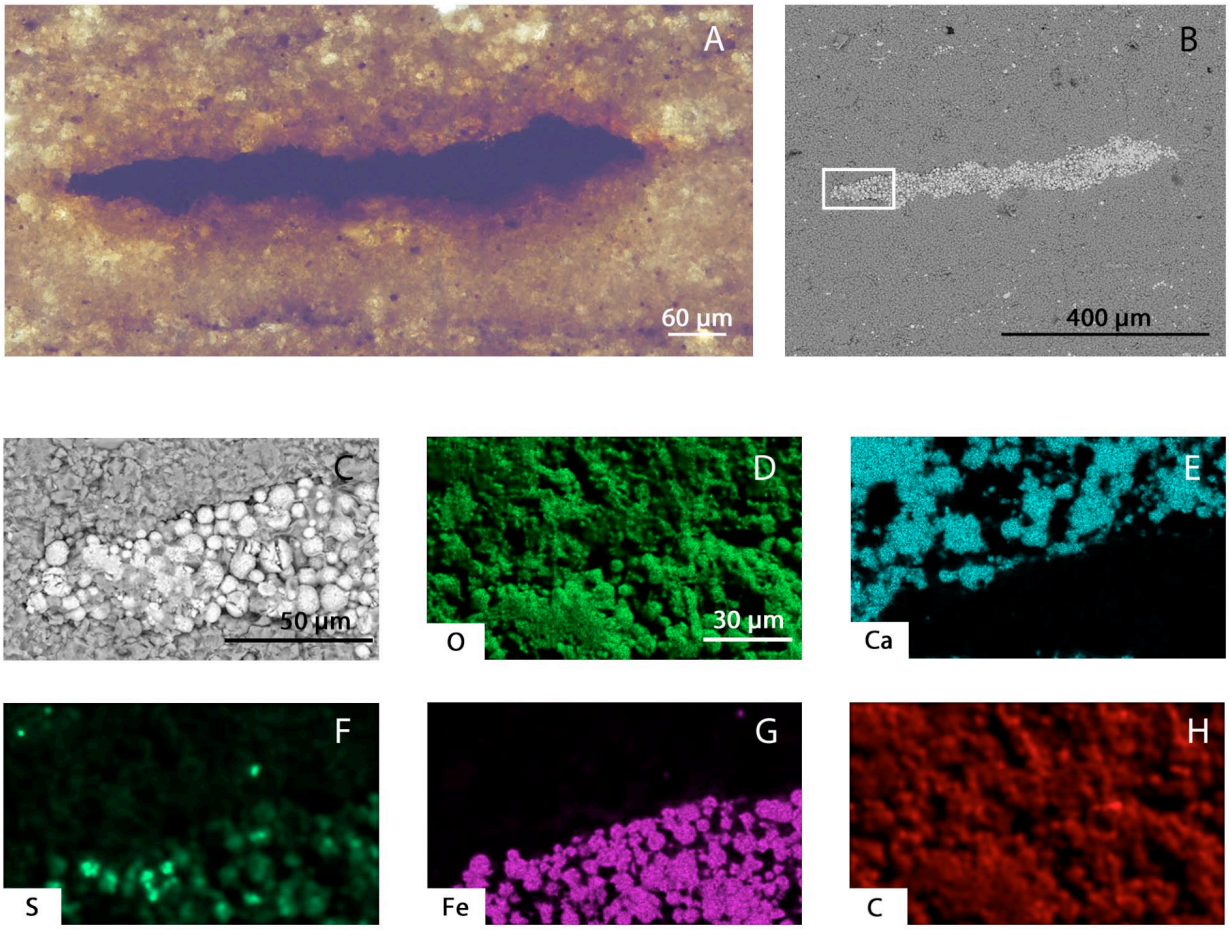

Figure 15- Transmitted Light Photomicrograph (A), BSE images (B-C), and elemental maps (D-H) of a small *Chuaria* fossil in cross section (SFT-15-2-#9), from Sifangtan. A: Image of the whole fossil. B: Another image of the whole fossil. The white box indicates the area shown in (C). C: Close-up image of the fossil's left margin showing framboids. Images (D-H) are elemental maps of the area in (C). Scale present in (D) applies for (E-H).

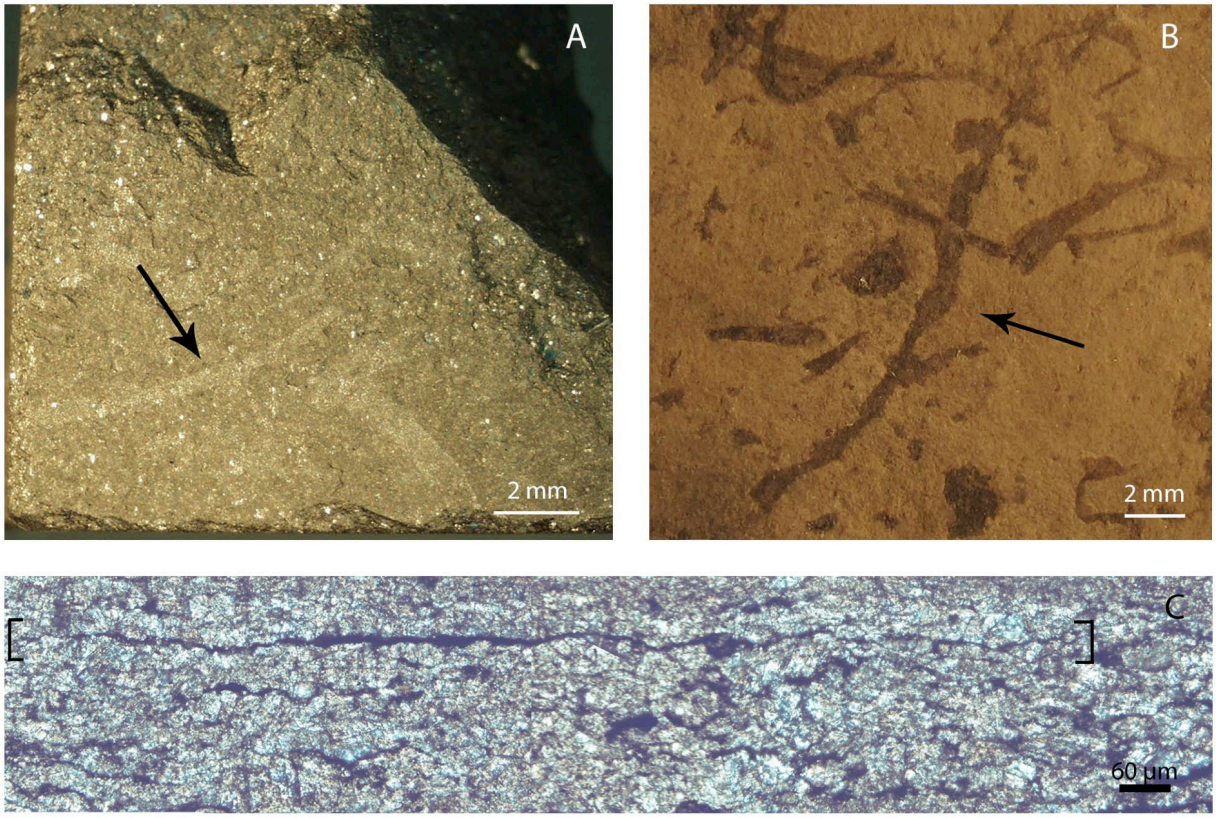

Figure 16- Reflected Light Photomicrographs (A-B) and Transmitted Light Photomicrographs (C) of specimens of *Vendotaenia* in both plane view (A-B) and cross section (C). Examples of *Vendotaenia* specimens in plane view are marked by arrows. A: Freshly exposed sample with multiple *Vendotaenia* specimens from the Wuhe section, sample number SBT-9. B: Sample from the Miaohe section with numerous *Vendotaenia* fossils on highly weathered siltstone, sample number MH-6. C: Probable fossil of *Vendotaenia* in cross-section (SBT-9-#2), from Wuhe. The black brackets demark the right and left edges of the fossil.

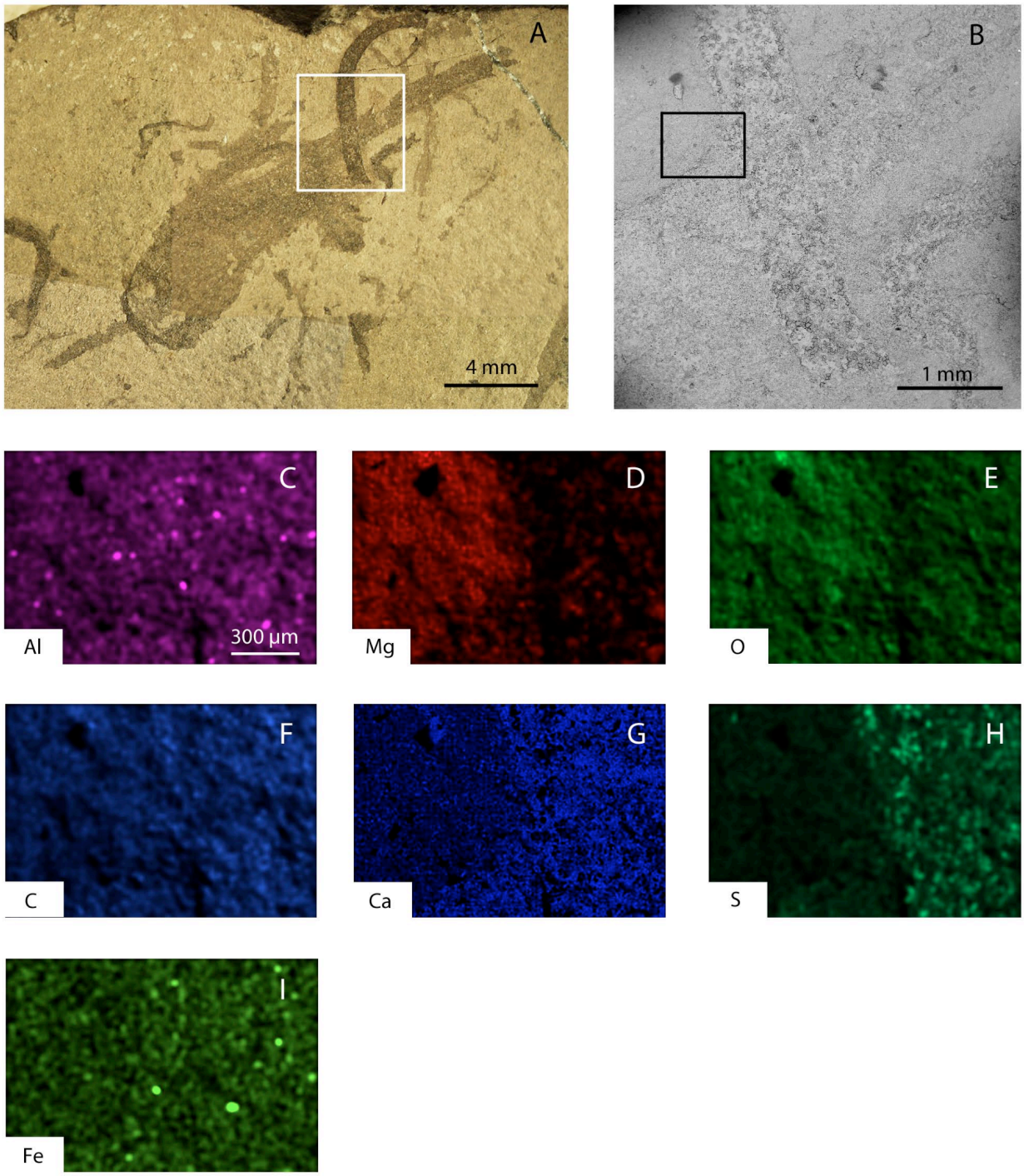

Figure 17- Reflected Light Photomicrograph (A), BSE image (B), and elemental maps (C-I) of a cluster of *Vendotaenia* fossils intersecting a stain on bedding plane (MH-7-#1), from Miaohe. A: Photograph of the entire specimen. The white box marks the area shown in (B). B: The intersection of two *Vendotaenia* ribbons and the "stain." (C-I) are elemental maps of the area indicated by the black box in (B). Scale present in (C) applies elemental maps (D-I).

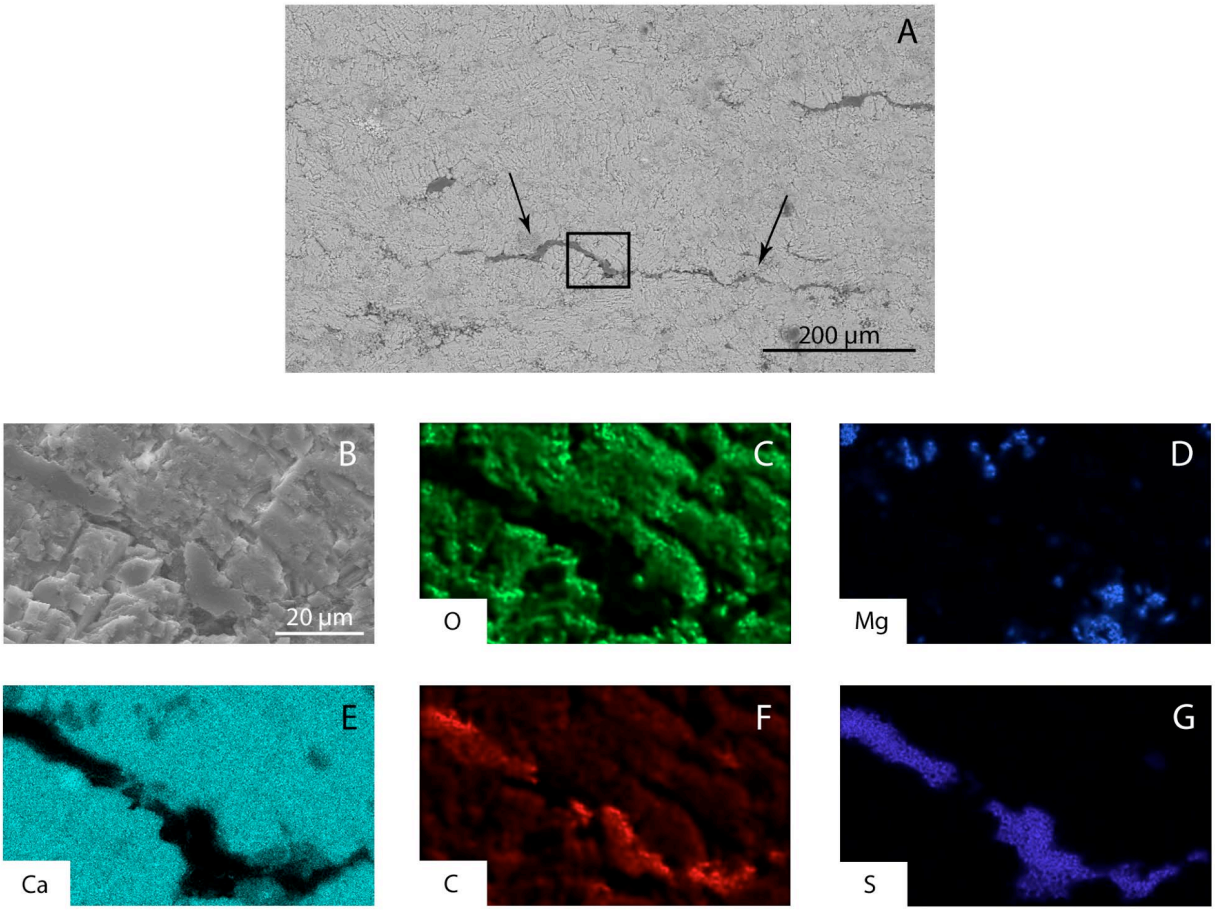

Figure 18- BSE image (A), SE image (B), and elemental maps (C-G) of a *Vendotaenia* fossil in cross-section (SBT-9-#3), from Wuhe. A: Image of the whole fossil. Note the low brightness of the carbonaceous compression as indicated by the arrows. There is probably another *Vendotaenia* fossil in the upper right corner of the image. The small black box marks the area shown and analyzed in (B-G). Close-up image of the fossil. The fossil can be seen running from the upper left to lower right. This was the area of analysis for elemental maps (C-G). Scale in (B) applies to (C-G).

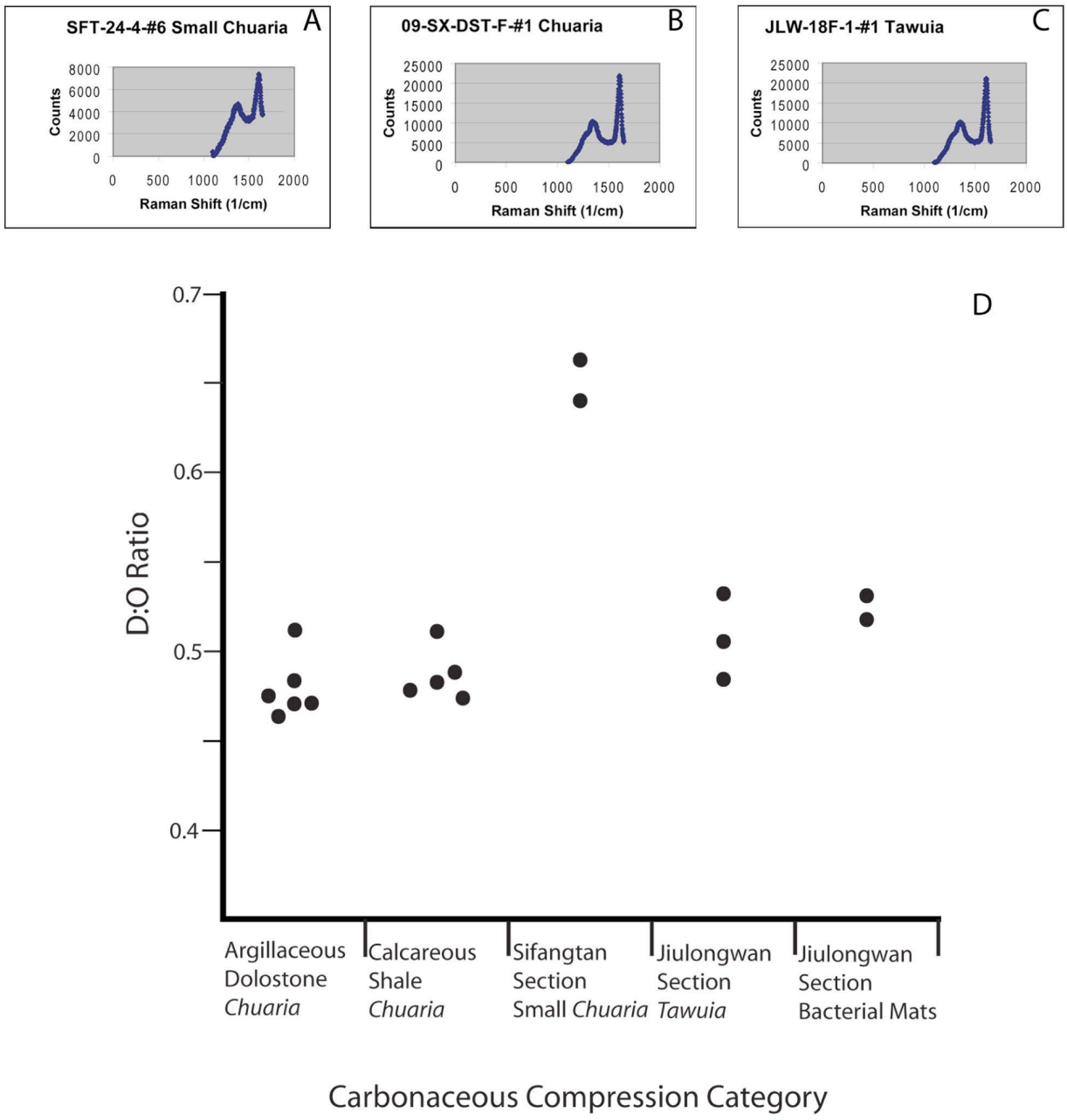

Figure 19- Representative RAMAN spectra and D:G ratios of carbonaceous compressions from the Doushantuo Formation. A: RAMAN spectra for a small *Chuaria* fossil (SFT-24-4-#6), from Sifangtan. B: RAMAN spectra for a *Chuaria* specimen (09-SX-DST-F-#1), from the calcareous siltstone lithology of the Sixi section. C: RAMAN spectra for a *Tawuia* specimen, (JLW-18F-1-#1) from the calcareous siltstone lithology of the lower Member II at the Jiulongwan section. D: Graph showing the D:G ratio for different groups of carbonaceous compressions. The D:G ratio is a relative measure of thermal maturiy: greater D:G ratios indicate lower thermal maturity. Points are scattered for ease of observation.

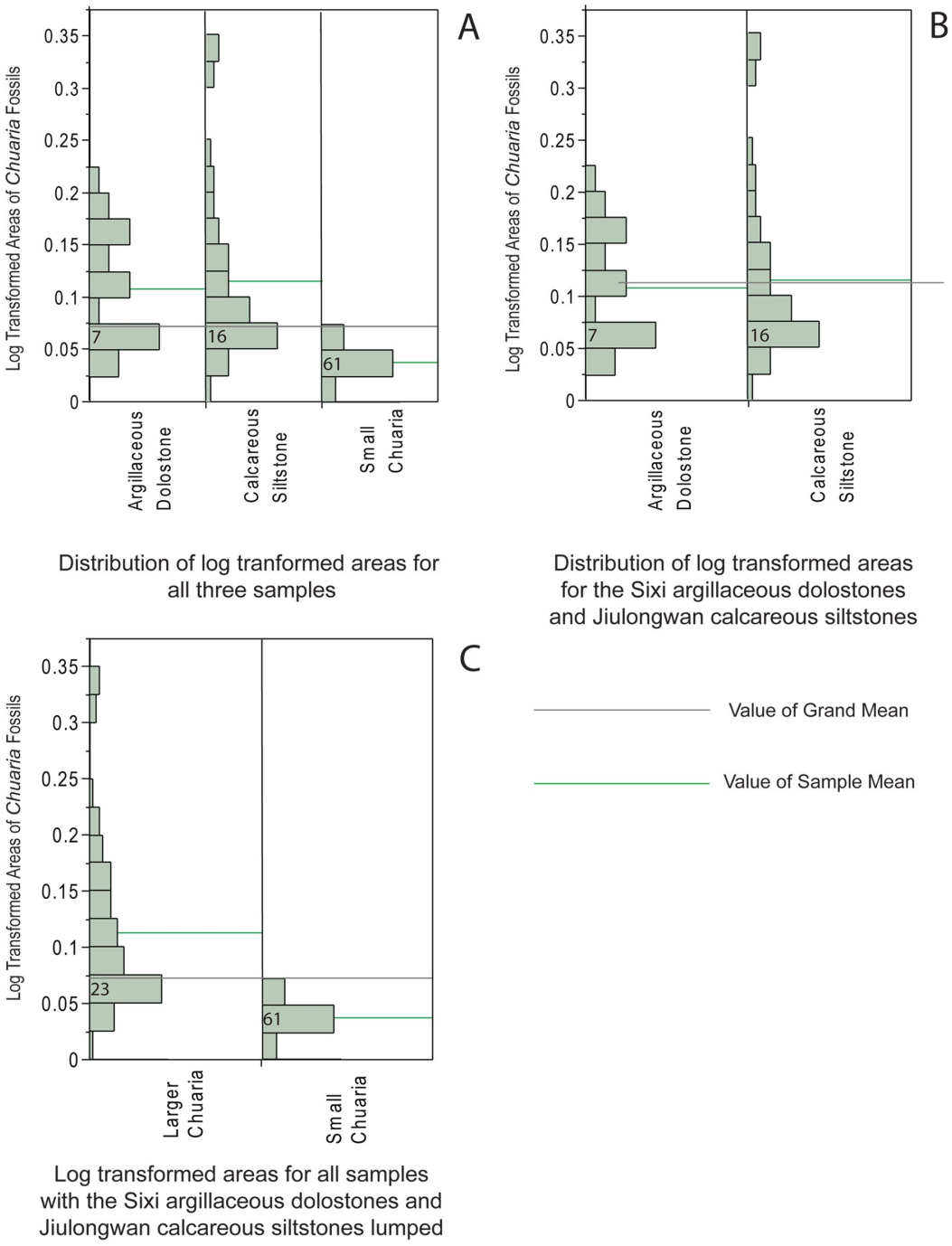

Figure 20- Plots showing the relative distribuiton of log transformed areas for three samples of *Chuaria*. One sample consists of the *Chuaria* specimens from the argillaceous dolostone lithology of the Sixi section, another of the *Chuaria* specimens from the calcareous siltstones of lower Member II at the Jiulongwan section, and the third consists of the small *Chuaria* from the Sifangtan and upper Jiulongwan sections. A: All three samples. B: The larger *Chuaria* specimens from the Sixi and lower member II Jiulongwan sections. C: All specimens, but with the larger *Chuaria* from the Sixi and lower Member II Jiulongwan sections lumped together as one sample. Gray lines are the grand mean, orange lines are the sample mean. The number in the largest bin of each histogram indicates the number of log transformed areas in that bin.

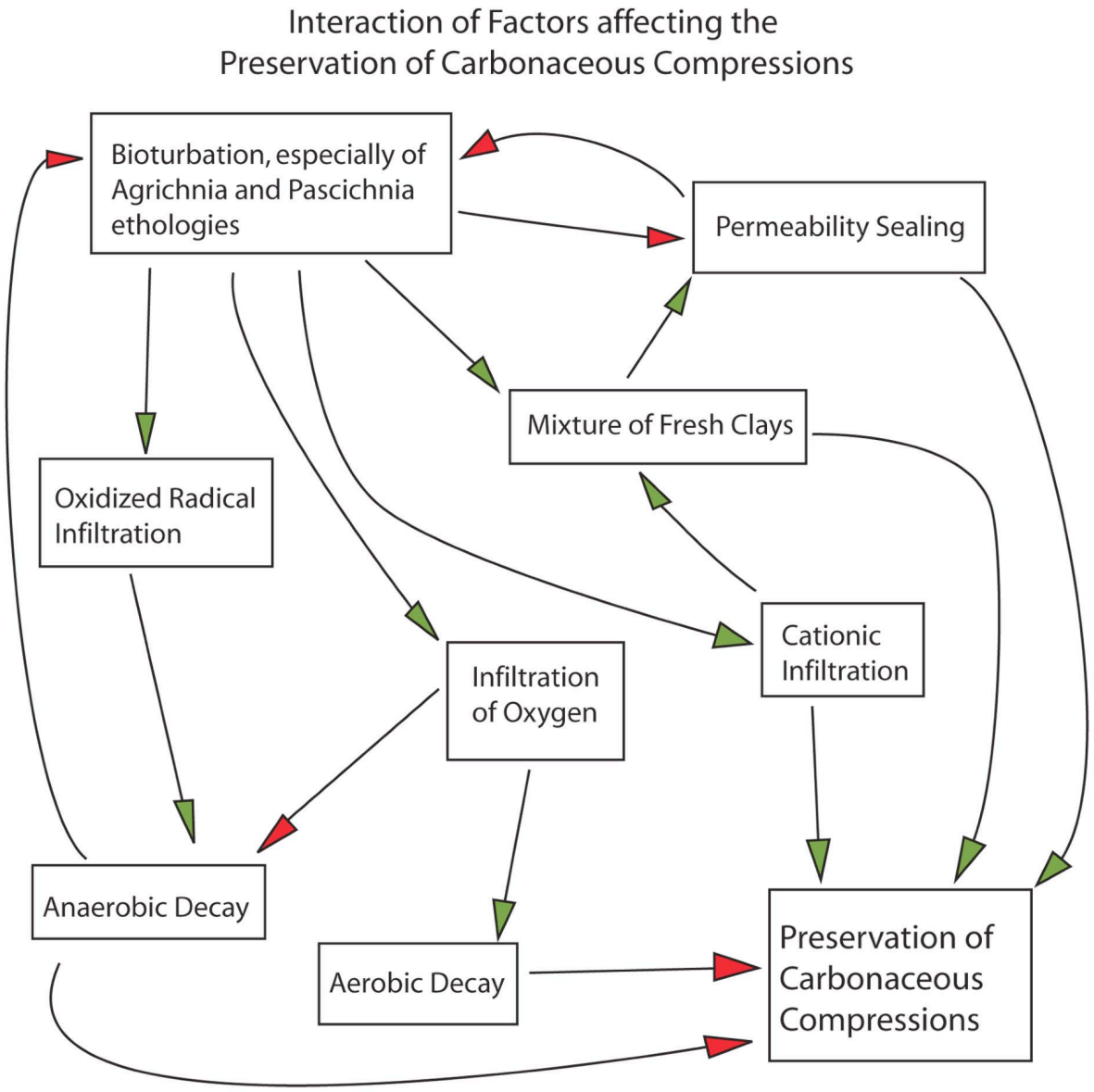

Figure 21- A diagram detailing the relationships of various burial and early diagenetic factors affecting the preservation of carbonaceous compressions. Green arrow heads indicate positive couplings. Red arrowheads represent negative couplings. For simplicity's sake, neither all factors nor all relationships could be included in this diagram.

Table 1- Point analysis of elemental abundances in carbonaceous compressions and their surrounding matrix. Not all elements present were necessarily analyzed, so some percentages may not add up to 100%

Sample/Specimen	Location	C(wt%)	O(wt%)	Mg(wt%)	Al(wt%)	Si(wt%)	S(wt%)	Ca(wt%)	Fe (wt%)
SFT-24-1	Matrix	9.9	52.5	11.1	0.5	1.0	N/A	14.6	2.4
SBT-9-#3	small *Chuaria*	23.8	63.8	0.8	0.0	6.0	N/A	5.1	0.5
SBT-9	Matrix	4.2	30.4	0.3	0.2	0.9	1.9	58.5	N/A
SBT-9-#3	*Vendotaenia*	61.3	24.7	0.1	0.0	0.0	13.0	0.8	N/A

Table 2- RAMAN data of specimens examined from the Doushantuo Formation, their lithology, and location of origin.

Fossil Type	Sample No.	Specimen No.	Lithology	Locality	D:G Ratio
Chuaria	09-SX-DST-A-5	#1	Argillaceous Dolostone	Sixi	0.4701
Chuaria	09-SX-DST-A-5	#1	Argillaceous Dolostone	Sixi	0.4704
Chuaria	09-SX-DST-A-5	#1	Argillaceous Dolostone	Sixi	0.5113
Chuaria	09-SX-DST-A-5	#2	Argillaceous Dolostone	Sixi	0.4755
Chuaria	09-SX-DST-A-5	#2	Argillaceous Dolostone	Sixi	0.4873
Chuaria	09-SX-DST-A-5	#2	Argillaceous Dolostone	Sixi	0.4639
Chuaria	09-SX-DST-A-5	#2	Argillaceous Dolostone	Sixi	0.4831
Bacterial Mat	JLW-F10-2	#1	Calcareous Siltstone	Jiulongwan	0.5309
Bacterial Mat	JLW-F10-2	#1	Calcareous Siltstone	Jiulongwan	0.5189
Chuaria	JLW-18E-1	#1	Calcareous Siltstone	Jiulongwan	0.4832
Chuaria	JLW-18E-1	#1	Calcareous Siltstone	Jiulongwan	0.4895
Chuaria	JLW-18E-1	#1	Calcareous Siltstone	Jiulongwan	0.4794
Chuaria	09-SX-DST-F	#2	Calcareous Siltstone	Sixi	0.4742
Chuaria	09-SX-DST-F	#1	Calcareous Siltstone	Sixi	0.5113
Small *Chuaria*	SFT-24-4	#6	Argillaceous Dolostone	Sifangtan	0.6403
Small *Chuaria*	SFT-24-4	#7	Argillaceous Dolostone	Sifangtan	0.663
Tawuia	JLW-18F-1	#1	Calcareous Siltstone	Jiulongwan	0.5326
Tawuia	JLW-18F-1	#1	Calcareous Siltstone	Jiulongwan	0.5062
Tawuia	JLW-18F-1	#1	Calcareous Siltstone	Jiulongwan	0.4855

Table 3- Means and sample sizes for the three populations of *Chuaria* sampled in the Doushantuo formation. The three samples are listed in the uppermost row. In some instances, only one or another axis of a *Chuaria* specimen could be measured, giving different sample sizes for some means.

Means and Sample Sizes	Sixi Argillaceous Dolostone (A)	Lower Member II Jiulongwan Section Calcareous Siltstone (B)	Small *Chuaria* (Sifangtan and Upper Member II Jiulongwan Section (C)
Axis 1 (mm)	1.5	1.62	0.71
Axis 1 (n=)	26	56	92
Axis 2 (mm)	1.16	1.25	0.6
Axis 2 (n=)	27	56	92
Surface Area (mm^2)	1.63	2.09	0.35
Log Transformed Surface Area	0.108	0.116	0.038
Area (n=)	24	55	92

Table 4- Statistical ummary of the data presented in Fig. 20. Population A is from the argillaceous dolostone of the Sixi section, Population B is from the calcareous siltstone of the lower Member II at Jiulongwan section, and Population C consists of the small *Chuaria* fossils from the Sifangtan and upper Member II at Jiulongwan sections (see also Table 3).

ANOVA Test	F-statistic	p-value
A vs. B vs. C	44.02	<.0001
A vs. B	0.19	0.66
A+B vs. C	87.95	<0.001

APPENDIX

Table A1. Samples and Specimens used for this study.

Sample No.	Collection Date	Location	Lithology	Specimen No.	Taxon	Orientation	Appendix A1 Photo No.	Appendix A2 SE Image No.	Appendix A2 BSE Image No.	Appendix A3 Elemental Maps	Raman microspectroscopy	Biometric Analysis
08-SX-DST3-3A1	2008	Sixi	Argillaceous Dolostone	N/A	N/A	N/A	N	N	N	-	N	N
08-SX-DST3-3A2	2008	Sixi	Argillaceous Dolostone	N/A	N/A	N/A	N	N	N	-	N	N
08-SX-DST3-3A3	2008	Sixi	Argillaceous Dolostone	N/A	N/A	XS	189, 190, 204	N	N	-	N	N
.	.	.	.	1	*Chuaria?*	XS	187, 188	N	N	-	N	N
.	.	.	.	2	*Chuaria*	XS	191, 192, 193	N	N	-	N	N
.	.	.	.	3	Carbonaceous Piece	XS	194, 195, 196, 197, 198	N	N	-	N	N
.	.	.	.	4	Carbonaceous Piece	XS	199	N	N	-	N	N
.	.	.	.	5	*Chuaria*	XS	200, 201	N	N	-	N	N
.	.	.	.	6	*Chuaria?*	XS	202	N	N	-	N	N
.	.	.	.	7	Carbonaceous Compression?	XS	203	N	N	-	N	N
08-SX-DST3-3A4	2008	Sixi	Argillaceous Dolostone	N/A	N/A	N/A	N	N	N	-	N	N
08-SX-DST3-3A5	2008	Sixi	Argillaceous Dolostone	N/A	N/A	N/A	N	N	N	-	N	N
08-SX-DST3-3A6	2008	Sixi	Argillaceous Dolostone	N/A	N/A	N/A	N	N	N	-	N	N
08-SX-DST3-3A7	2008	Sixi	Argillaceous Dolostone	N/A	N/A	N/A	N	N	N	-	N	N
08-SX-DST3-3B1	2008	Sixi	Argillaceous Dolostone	N/A	N/A	BP	13, 15, 17, 18	N	N	-	N	N
.	.	.	.	1	*Chuaria*	BP	11	N	N	-	N	N
.	.	.	.	2	*Chuaria*	BP	11	N	N	-	N	N
.	.	.	.	3	*Chuaria*	BP	11	N	N	-	N	N
.	.	.	.	4	*Tawuia*	BP	12	N	N	-	N	N
.	.	.	.	5	*Chuaria*	BP	14	N	N	-	N	N
.	.	.	.	6	*Chuaria*	BP	14	N	N	-	N	N
.	.	.	.	7	*Chuaria*	BP	14	N	N	-	N	N
.	.	.	.	8	*Chuaria*	BP	16	N	N	-	N	N
08-SX-DST3-3B2	2008	Sixi	Argillaceous Dolostone	N/A	N/A	N/A	N	N	N	-	N	N
08-SX-DST3-3B3	2008	Sixi	Argillaceous Dolostone	N/A	N/A	N/A	N	N	N	-	N	N
.	.	.	.	1	*Chuaria*	BP	19	N	N	-	N	N
.	.	.	.	2	*Tawuia*	BP	20, 42	N	N	-	N	N
.	.	.	.	3	*Chuaria*	BP	20, 42	N	N	-	N	N

.	.	.	.	4	*Chuaria*	BP	20, 42	N	N	-	N	N
.	.	.	.	5	*Chuaria*	BP	21, 41	N	1, 2, 3	Al, Mg, Si, Ca, C, P, Fe	N	N
08-SX-DST3-3B4	2008	Sixi	Argillaceous Dolostone	N/A	N/A	N/A	N	N	N	-	N	N
08-SX-DST3-3C	2008	Sixi	Argillaceous Dolostone	N/A	N/A	BP	22	N	N	-	N	N
.	.	.	.	1	*Chuaria*	BP	23	N	N	-	N	N
.	.	.	.	2	*Chuaria*	BP	114	N	N	-	N	Y
.	.	.	.	3	*Chuaria*	BP	115	N	N	-	N	N
.	.	.	.	4	*Chuaria*	BP	116	N	N	-	N	N
.	.	.	.	5	*Chuaria*	BP	117	N	N	-	N	Y
.	.	.	.	6	*Chuaria*	BP	117	N	N	-	N	Y
.	.	.	.	7	*Chuaria*	BP	118	N	N	-	N	Y
.	.	.	.	8	*Chuaria*	BP	119	N	N	-	N	Y
.	.	.	.	9	*Chuaria*	BP	120	N	N	-	N	N
.	.	.	.	10	*Chuaria*	BP	121	N	N	-	N	Y
.	.	.	.	11	*Chuaria*	BP	122	N	N	-	N	Y
.	.	.	.	12	*Chuaria*	BP	123	N	N	-	N	Y
.	.	.	.	13	*Chuaria*	BP	124	N	N	-	N	Y
.	.	.	.	14	*Chuaria*	BP	125	N	N	-	N	Y
.	.	.	.	15	*Chuaria*	BP	126	N	N	-	N	Y
.	.	.	.	16	*Chuaria*	BP	127	N	N	-	N	Y
.	.	.	.	17	*Chuaria*	BP	127	N	N	-	N	Y
.	.	.	.	18	*Tawuia*	BP	128	N	N	-	N	Y
.	.	.	.	19	*Tawuia*	BP	129	N	N	-	N	Y
.	.	.	.	20	*Chuaria*	BP	130	N	N	-	N	Y
.	.	.	.	21	*Chuaria*	BP	131	N	N	-	N	Y
.	.	.	.	22	*Chuaria*	BP	132	N	N	-	N	Y
.	.	.	.	23	*Chuaria*	BP	133	N	N	-	N	Y
.	.	.	.	24	*Chuaria*	BP	134	N	N	-	N	Y
.	.	.	.	25	*Chuaria*	BP	135	N	N	-	N	Y
.	.	.	.	26	*Chuaria*	BP	135	N	N	-	N	N
.	.	.	.	27	*Tawuia*	BP	136	N	N	-	N	Y
.	.	.	.	28	*Chuaria*	BP	136	N	N	-	N	Y
.	.	.	.	29	*Chuaria*	BP	136	N	N	-	N	Y
.	.	.	.	30	*Chuaria*	BP	137	N	N	-	N	Y
.	.	.	.	31	*Chuaria*	BP	138	N	N	-	N	Y
.	.	.	.	32	*Tawuia*	BP	139	N	N	-	N	Y
.	.	.	.	33	*Chuaria*	BP	139	N	N	-	N	Y
.	.	.	.	34	*Chuaria*	BP	140	N	N	-	N	Y
.	.	.	.	35	*Chuaria*	BP	141	N	N	-	N	Y
.	.	.	.	36	*Chuaria*	BP	141	N	N	-	N	Y
.	.	.	.	37	*Chuaria*	BP	142	N	N	-	N	Y
08-SX-DST3-3D1a	2008	Sixi	Argillaceous Dolostone	N/A	N/A	N/A	N	N	N	-	N	N

08-SX-DST3-3D1b	2008	Sixi	Argillaceous Dolostone	N/A	N/A	N/A	N	N	N	-	N	N
08-SX-DST3-3D1c	2008	Sixi	Argillaceous Dolostone	N/A	N/A	XS	3, 4, 5, 9, 33	N	N	-	N	N
.	.	.	.	1	*Chuaria*	XS	1	N	N	-	N	N
.	.	.	.	2	*Chuaria*	XS	1	N	N	-	N	N
.	.	.	.	3	*Chuaria*	XS	2	N	N	-	N	N
.	.	.	.	4	*Chuaria*	XS	6	N	N	-	N	N
.	.	.	.	5	*Chuaria*	XS	6, 8	N	N	-	N	N
.	.	.	.	6	*Chuaria*	XS	7	N	N	-	N	N
.	.	.	.	7	*Chuaria*	XS	32	N	N	-	N	N
.	.	.	.	8	*Chuaria*	XS	34	N	N	-	N	N
08-SX-DST3-3D1d	2008	Sixi	Argillaceous Dolostone	N/A	N/A	N/A	N	N	N	-	N	N
08-SX-DST3-3D1e	2008	Sixi	Argillaceous Dolostone	N/A	*N/A*	N/A	N	N	N	-	N	N
.	.	.	.	1	*Chuaria*	XS	269, 270, 271	6, 8, 9	4, 5, 7	Al, Mg, Si, O, Ca, C, P, S, Fe, K, F	N	N
.	.	.	.	2	*Chuaria*	XS	N	11	10	Al, Mg, Si, O, Ca, C, P, S, Fe, K	N	N
.	.	.	.	3	*Chuaria?*	XS	N	14	12, 13	Mg, Si, O, Ca, C, P	N	N
08-SX-DST3-3D1f	2008	Sixi	Argillaceous Dolostone	N/A	N/A	N/A	N	N	N	-	N	N
08-SX-DST3-3D1g	2008	Sixi	Argillaceous Dolostone	N/A	N/A	N/A	N	N	N	-	N	N
08-SX-DST3-3D2	2008	Sixi	Argillaceous Dolostone	N/A	N/A	N/A	N	N	N	-	N	N
08-SX-DST3-3D3	2008	Sixi	Argillaceous Dolostone	N/A	N/A	N/A	N	N	N	-	N	N
08-SX-DST3-3D4	2008	Sixi	Argillaceous Dolostone	N/A	N/A	N/A	N	N	N	-	N	N
08-SX-DST3-3D5	2008	Sixi	Argillaceous Dolostone	N/A	N/A	N/A	N	N	N	-	N	N
08-SX-DST3-3D6	2008	Sixi	Argillaceous Dolostone	N/A	N/A	N/A	N	N	N	-	N	N
08-SX-DST3-3E1a	2008	Sixi	Argillaceous Dolostone	N/A	N/A	N/A	N	N	N	-	N	N
.	.	.	.	1	*Chuaria?*	BP	35, 39	N	N	-	N	N
.	.	.	.	2	*Chuaria*	BP	35, 39	N	N	-	N	N
.	.	.	.	3	*Chuaria*	BP	35, 39	N	N	-	N	N
.	.	.	.	4	Carbonaceous Piece	BP	39	15	N	Al, Mg, Si, O, Ca, C, P, S, Fe, K	N	N
08-SX-DST3-3E1b	2008	Sixi	Argillaceous Dolostone	N/A	N/A	N/A	N	N	N	-	N	N
.	.	.	.	1	*Chuaria*	BP	36, 40	N	16, 17	Al, Mg, Si, O, Ca, C, P, S, Fe, K	N	N
.	.	.	.	2	*Chuaria*	BP	36, 40	N	N	-	N	N
08-SX-DST3-3E1c	2008	Sixi	Argillaceous Dolostone	N/A	N/A	N/A	N	N	N	-	N	N
08-SX-DST3-3E1d	2008	Sixi	Argillaceous Dolostone	N/A	N/A	N/A	N	N	N	-	N	N
.	.	.	.	1	*Chuaria?*	BP	37, 38	N	18	-	N	N

08-SX-DST3-3E2	2008	Sixi	Argillaceous Dolostone	N/A	N/A	BP	26	N	N	-	N	N
.	.	.	.	1	Carbonaceous Piece	BP	24	N	N	-	N	N
.	.	.	.	2	*Chuaria*	BP	24	N	N	-	N	N
.	.	.	.	3	*Chuaria*	BP	25	N	N	-	N	N
.	.	.	.	4	*Chuaria*	BP	27	N	N	-	N	N
.	.	.	.	5	*Chuaria*	BP	27	N	N	-	N	N
.	.	.	.	6	*Chuaria*	BP	28	N	N	-	N	N
.	.	.	.	7	*Chuaria*	BP	29	N	N	-	N	N
.	.	.	.	8	*Chuaria*	BP	30	N	N	-	N	N
.	.	.	.	9	Carbonaceous Piece	BP	31	N	N	-	N	N
08-SX-DST3-3E3	2008	Sixi	Argillaceous Dolostone	N/A	N/A	N/A	N	N	N	-	N	N
JLW-18A	2005	Jiulongwan	Calcareous Siltstone	N/A	N/A	N/A	N	N	N	-	N	N
.	.	.	.	1	chuaroid	BP	10	N	N	-	N	N
JLW-18B	2005	Jiulongwan	Calcareous Siltstone	N/A	N/A	N/A	N	N	N	-	N	N
.	.	.	.	1	*Chuaria*	BP	52	N	N	-	N	Y
.	.	.	.	2	*Chuaria*	BP	53	N	N	-	N	Y
.	.	.	.	3	*Chuaria*	BP	54	N	N	-	N	Y
.	.	.	.	4	*Chuaria*	BP	54	N	N	-	N	Y
.	.	.	.	5	*Chuaria*	BP	55	N	N	-	N	Y
.	.	.	.	6	*Chuaria*	BP	56	N	N	-	N	Y
.	.	.	.	7	*Chuaria*	BP	57	N	N	-	N	Y
.	.	.	.	8	*Tawuia*	BP	58	N	N	-	N	Y
JLW-18C	2005	Jiulongwan	Calcareous Siltstone	N/A	N/A	N/A	N	N	N	-	N	N
.	.	.	.	1	*Chuaria*	BP	59	N	N	-	N	Y
.	.	.	.	2	*Chuaria*	BP	59	N	N	-	N	Y
.	.	.	.	3	*Chuaria*	BP	60	N	N	-	N	Y
.	.	.	.	4	*Chuaria*	BP	61	N	N	-	N	Y
.	.	.	.	5	*Chuaria*	BP	62	N	N	-	N	Y
.	.	.	.	6	*Chuaria*	BP	63	N	N	-	N	Y
.	.	.	.	7	*Chuaria*	BP	64	N	N	-	N	Y
.	.	.	.	8	*Chuaria*	BP	65	N	N	-	N	Y
.	.	.	.	9	*Tawuia*	BP	66	N	N	-	N	Y
.	.	.	.	10	*Chuaria*	BP	67	N	N	-	N	Y
.	.	.	.	11	*Chuaria*	BP	68	N	N	-	N	Y
.	.	.	.	12	*Chuaria*	BP	69	N	N	-	N	Y
.	.	.	.	13	*Chuaria*	BP	70	N	N	-	N	Y
JLW-18D	2005	Jiulongwan	Calcareous Siltstone	N/A	N/A	N/A	N	N	N	-	N	N
.	.	.	.	1	*Chuaria*	BP	71	N	N	-	N	Y
.	.	.	.	2	*Chuaria*	BP	72	N	N	-	N	Y
.	.	.	.	3	*Chuaria*	BP	73	N	N	-	N	Y
.	.	.	.	4	*Chuaria*	BP	74	N	N	-	N	Y

.	.	.	.	5	*Chuaria*	BP	75	N	N	-	N	Y
.	.	.	.	6	*Chuaria*	BP	76	N	N	-	N	Y
.	.	.	.	7	*Chuaria*	BP	77	N	N	-	N	Y
.	.	.	.	8	*Chuaria*	BP	78	N	N	-	N	Y
.	.	.	.	9	*Tawuia*	BP	79	N	N	-	N	Y
.	.	.	.	10	*Chuaria*	BP	80	N	N	-	N	Y
.	.	.	.	11	*Chuaria*	BP	81	N	N	-	N	Y
.	.	.	.	12	*Chuaria*	BP	82	N	N	-	N	Y
.	.	.	.	13	*Chuaria*	BP	85	N	N	-	N	Y
.	.	.	.	14	*Chuaria*	BP	86	N	N	-	N	Y
.	.	.	.	15	*Chuaria*	BP	87	N	N	-	N	Y
.	.	.	.	16	*Chuaria*	BP	88	N	N	-	N	Y
.	.	.	.	17	*Chuaria*	BP	89	N	N	-	N	N
.	.	.	.	18	*Chuaria*	BP	90	N	N	-	N	Y
.	.	.	.	19	*Chuaria*	BP	91	N	N	-	N	Y
.	.	.	.	20	*Chuaria*	BP	92	N	N	-	N	Y
.	.	.	.	21	*Chuaria*	BP	92	N	N	-	N	Y
.	.	.	.	22	*Chuaria*	BP	93	N	N	-	N	Y
.	.	.	.	23	*Tawuia?*	BP	83	N	N	-	N	N
.	.	.	.	24	*Tawuia?*	BP	84	N	N	-	N	N
JLW-18E	2005	Jiulongwan	Calcareous Siltstone	N/A	N/A	N/A	N	N	N	-	N	N
.	.	.	.	1	*Chuaria*	BP	94	N	N	-	N	Y
.	.	.	.	2	*Chuaria*	BP	95	N	N	-	N	Y
.	.	.	.	3	*Chuaria*	BP	96	N	N	-	N	Y
.	.	.	.	4	*Chuaria*	BP	97	N	N	-	N	Y
.	.	.	.	5	*Chuaria*	BP	98, 162	N	N	-	Y	Y
JLW-18F	2005	Jiulongwan	Calcareous Siltstone	N/A	N/A	N/A	N	N	N	-	N	N
.	.	.	.	1	*Tawuia*	BP	44, 45, 46, 99	24	19, 20, 21, 22, 23	Al, Mg, Si, O, Ca, C, Fe, K, Na	Y	Y
JLW-18G	2005	Jiulongwan	Calcareous Siltstone	N/A	N/A	BP	47, 112	N	N	-	N	N
.	.	.	.	1	*Chuaria*	BP	100, 170	N	N	-	N	Y
.	.	.	.	2	*Chuaria*	BP	49, 101, 170, 171, 172	N	N	-	N	Y
.	.	.	.	3	*Chuaria*	BP	102, 170, 171, 172	N	N	-	N	Y
.	.	.	.	4	*Chuaria*	BP	48, 103, 170, 171	N	N	-	N	Y
.	.	.	.	5	*Chuaria*	BP	48, 103, 170, 171	N	N	-	N	Y
.	.	.	.	6	*Chuaria*	BP	48, 104, 170, 171	N	N	-	N	Y
.	.	.	.	7	*Chuaria*	BP	48, 105, 170, 171	N	N	-	N	N
.	.	.	.	8	*Tawuia*	BP	106, 170, 171	N	N	-	N	Y
.	.	.	.	9	*Chuaria*	BP	107	N	N	-	N	Y

.	.	.	.	10	*Chuaria*	BP	107	N	N	-	N	Y
.	.	.	.	11	*Chuaria*	BP	108	N	N	-	N	Y
.	.	.	.	12	*Chuaria*	BP	109	N	N	-	N	Y
.	.	.	.	13	*Chuaria*	BP	110	N	N	-	N	Y
.	.	.	.	14	*Chuaria*	BP	110	N	N	-	N	Y
.	.	.	.	15	*Chuaria*	BP	110	N	N	-	N	Y
.	.	.	.	16	*Chuaria*	BP	110	N	N	-	N	Y
.	.	.	.	17	*Chuaria*	BP	111	N	N	-	N	Y
.	.	.	.	18	*Tawuia*	BP	50, 113	N	N	-	N	Y
.	.	.	.	19	*Chuaria*	BP	51	N	N	-	N	N
JLW-27Aa	2005	Jiulongwan	Calcareous Siltstone	N/A	N/A	N/A	N	N	N	-	N	N
JLW-27Ab	2005	Jiulongwan	Calcareous Siltstone	N/A	N/A	N/A	N	N	N	-	N	N
JLW-27Ac	2005	Jiulongwan	Calcareous Siltstone	N/A	N/A	N/A	N	N	N	-	N	N
JLW-27Ad	2005	Jiulongwan	Calcareous Siltstone	N/A	N/A	N/A	N	N	N	-	N	N
JLW-27Ae	2005	Jiulongwan	Calcareous Siltstone	N/A	N/A	N/A	N	N	N	-	N	N
JLW-27Af	2005	Jiulongwan	Calcareous Siltstone	N/A	N/A	N/A	N	N	N	-	N	N
.	.	.	.	1	*Chuaria*	BP	43	N	25	Al, Mg, Si, O, Ca, C, P, S, Fe, K	N	N
.	.	.	.	2	Calcite Chip	BP	43	N	26, 27	Al, Mg, Si, O, Ca, C, P, S, Fe, K	N	N
JLW-F10-1	2009	Jiulongwan	Calcareous Siltstone	N/A	N/A	BP, XS	152, 153, 154	N	28	-	N	N
.	.	.	.	1	Bacteria Sheet	BP, XS	173, 174, 175, 176, 177, 178	30	29	-	N	Y
JLW-F10-2	2009	Jiulongwan	Calcareous Siltstone	N/A	N/A	BP	155, 156	N	N	-	N	N
JLW-F10-3	2009	Jiulongwan	Calcareous Siltstone	N/A	N/A	N/A	N	N	N	-	N	N
JLW-10-1	2009	Jiulongwan	Calcareous Siltstone	N/A	N/A	N/A	N	N	N	-	N	N
JLW-30-1	2009	Jiulongwan	Calcareous Siltstone	N/A	N/A	N/A	N	N	N	-	N	N
JLW-30-2	2009	Jiulongwan	Calcareous Siltstone	N/A	N/A	N/A	N	N	N	-	N	N
JLW-30-3	2009	Jiulongwan	Calcareous Siltstone	N/A	N/A	N/A	N	N	N	-	N	N
JLW-F-32 or 33	2009	Jiulongwan	Calcareous Siltstone	N/A	N/A	N/A	N	N	N	-	N	N
JLW-F-40-1	2009	Jiulongwan	Calcareous Siltstone	N/A	N/A	N/A	N	N	N	-	N	N
JLW-F-40-2	2009	Jiulongwan	Calcareous Siltstone	N/A	N/A	N/A	N	N	N	-	N	N
JLW-F-40-3	2009	Jiulongwan	Calcareous Siltstone	N/A	N/A	N/A	N	N	N	-	N	N
JLW-F-40-4	2009	Jiulongwan	Calcareous Siltstone	N/A	N/A	N/A	N	N	N	-	N	N
JLW-39.5-1	2009	Jiulongwan	Calcareous Siltstone	N/A	N/A	N/A	N	N	N	-	N	N

JLW-39.5-2	2009	Jiulongwan	Calcareous Siltstone	N/A	N/A	N/A	N	N	N	-	N	N
JLW-39.5-3	2009	Jiulongwan	Calcareous Siltstone	N/A	N/A	N/A	N	N	N	-	N	N
JLW-39.5-4	2009	Jiulongwan	Calcareous Siltstone	N/A	N/A	N/A	N	N	N	-	N	N
JLW-39.5-5	2009	Jiulongwan	Calcareous Siltstone	N/A	N/A	N/A	N	N	N	-	N	N
JLW-39.5-6	2009	Jiulongwan	Calcareous Siltstone	N/A	N/A	N/A	N	N	N	-	N	N
JLW-39.5-7	2009	Jiulongwan	Calcareous Siltstone	N/A	N/A	N/A	N	N	N	-	N	N
JLW-39.5-8	2009	Jiulongwan	Calcareous Siltstone	N/A	N/A	N/A	N	N	N	-	N	N
JLW-40-1	2009	Jiulongwan	Calcareous Siltstone	N/A	N/A	N/A	N	N	N	-	N	N
JLW-42.5-1	2009	Jiulongwan	Calcareous Siltstone	N/A	N/A	N/A	N	N	N	-	N	N
.	.	.	.	1	High Z Patch	XS	N	33	31, 32	-	N	N
JLW-42.5-2	2009	Jiulongwan	Calcareous Siltstone	N/A	N/A	N/A	N	N	N	-	N	N
JLW-42.5-3	2009	Jiulongwan	Calcareous Siltstone	N/A	N/A	N/A	N	N	N	-	N	N
JLW-42.5-4	2009	Jiulongwan	Calcareous Siltstone	N/A	N/A	N/A	N	N	N	-	N	N
.	.	.	.	1	Small *Chuaria*	BP	240	N	N	-	N	Y
.	.	.	.	2	Small *Chuaria*	BP	240	N	N	-	N	Y
.	.	.	.	3	Small *Chuaria*	BP	241	N	N	-	N	Y
.	.	.	.	4	Small *Chuaria*	BP	241	N	N	-	N	Y
.	.	.	.	5	Small *Chuaria*	BP	241	N	N	-	N	Y
.	.	.	.	6	Small *Chuaria*	BP	241	N	N	-	N	Y
.	.	.	.	7	Small *Chuaria*	BP	241	N	N	-	N	Y
.	.	.	.	8	Small *Chuaria*	BP	241	N	N	-	N	Y
.	.	.	.	9	Small *Chuaria*	BP	241	N	N	-	N	Y
.	.	.	.	10	Small *Chuaria*	BP	241	N	N	-	N	Y
.	.	.	.	11	Small *Chuaria*	BP	242	N	N	-	N	Y
.	.	.	.	12	Small *Chuaria*	BP	243	N	N	-	N	Y
.	.	.	.	13	Small *Chuaria*	BP	243	N	N	-	N	Y
.	.	.	.	14	Small *Chuaria*	BP	244	N	N	-	N	Y
.	.	.	.	15	Small *Chuaria*	BP	244	N	N	-	N	Y
.	.	.	.	16	Small *Chuaria*	BP	245	N	N	-	N	Y
JLW-F-40-5	2009	Jiulongwan	Calcareous Siltstone	N/A	N/A	N/A	N	N	N	-	N	N
JLW-57.5-1	2009	Jiulongwan	Calcareous Siltstone	N/A	N/A	N/A	N	N	N	-	N	N
JLW-57.5-2	2009	Jiulongwan	Calcareous Siltstone	N/A	N/A	N/A	N	N	N	-	N	N
JLW-57.5-3	2009	Jiulongwan	Calcareous Siltstone	N/A	N/A	N/A	N	N	N	-	N	N
SBT-1	2009	Wuhe	Limestone/Siltstone	N/A	N/A	N/A	N	N	N	-	N	N
SBT-2	2009	Wuhe	Limestone/Siltstone	N/A	N/A	N/A	N	N	N	-	N	N
SBT-3	2009	Wuhe	Limestone/Siltstone	N/A	N/A	BP, XS	179, 180, 181	N	N	-	N	N

SBT-4	2009	Wuhe	Limestone/Siltstone	N/A	N/A	N/A	N	N	N	-	N	N
SBT-5	2009	Wuhe	Limestone/Siltstone	N/A	N/A	N/A	N	N	N	-	N	N
SBT-6	2009	Wuhe	Limestone/Siltstone	N/A	N/A	N/A	N	N	N	-	N	N
SBT-7	2009	Wuhe	Limestone/Siltstone	N/A	N/A	N/A	N	N	N	-	N	N
SBT-8	2009	Wuhe	Limestone/Siltstone	N/A	N/A	N/A	N	N	N	-	N	N
SBT-9	2009	Wuhe	Limestone/Siltstone	N/A	N/A	BP, XS	248, 249, 259, 260, 262, 263, 267	N	N	-	N	N
.	.	.	.	1	*Vendotaenia*	XS	258	N	N	-	N	N
.	.	.	.	2	*Vendotaenia*	XS	261	N	N	-	N	N
.	.	.	.	3	*Vendotaenia*	XS	N	36	34, 35	Al, Mg, Si, O, Ca, C, S	N	N
SBT-10	2009	Wuhe	Limestone/Siltstone	N/A	N/A	N/A	N	N	N	-	N	N
SFT-F-1	2009	Sifangtan	Argillaceous Dolostone	N/A	N/A	N/A	N	N	N	-	N	N
SFT-12-1 F?	2009	Sifangtan	Argillaceous Dolostone	N/A	N/A	N/A	N	N	N	-	N	N
SFT-15-1	2009	Sifangtan	Argillaceous Dolostone	N/A	N/A	N/A	N	N	N	-	N	N
SFT-15-2	2009	Sifangtan	Argillaceous Dolostone	N/A	N/A	BP, XS	250, 251, 252, 265	N	N	-	N	N
.	.	.	.	1	Small *Chuaria*	BP	229	N	N	-	N	Y
.	.	.	.	2	Small *Chuaria*	BP	229	N	N	-	N	Y
.	.	.	.	3	Small *Chuaria*	BP	229	N	N	-	N	Y
.	.	.	.	4	Small *Chuaria*	BP	230	N	N	-	N	Y
.	.	.	.	5	Small *Chuaria*	BP	231	N	N	-	N	Y
.	.	.	.	6	Small *Chuaria*	BP	232	N	N	-	N	Y
.	.	.	.	7	Small *Chuaria*	BP	233	N	N	-	N	Y
.	.	.	.	8	Small *Chuaria*	BP	234	N	N	-	N	Y
.	.	.	.	9	Small *Chuaria*	XS	264	38, 40	37, 39	Al, Mg, Si, O, Ca, C, S, Fe	N	N
.	.	.	.	10	Small *Chuaria*	XS	266	N	N	-	N	N
.	.	.	.	11	Small *Chuaria*?	XS	N	41, 42	N	Al, Mg, Si, O, Ca, C, S, Fe	N	N
SFT-21-1	2009	Sifangtan	Argillaceous Dolostone	N/A	N/A	N/A	184, 185, 186	N	N	-	N	N
SFT-22-1	2009	Sifangtan	Argillaceous Dolostone	N/A	N/A	N/A	N	N	N	-	N	N
SFT-22-2	2009	Sifangtan	Argillaceous Dolostone	N/A	N/A	N/A	N	N	N	-	N	N
SFT-22-3	2009	Sifangtan	Argillaceous Dolostone	N/A	N/A	N/A	N	N	N	-	N	N
.	.	.	.	1	Small *Chuaria*	BP	235	N	N	-	N	Y
.	.	.	.	2	Small *Chuaria*	BP	235	N	N	-	N	Y
.	.	.	.	3	Small *Chuaria*	BP	235	N	N	-	N	Y
.	.	.	.	4	Small *Chuaria*	BP	235	N	N	-	N	Y
.	.	.	.	5	Small *Chuaria*	BP	236	N	N	-	N	Y

.	.	.	.	6	Small *Chuaria*	BP	237	N	N	-	N	Y
.	.	.	.	7	Small *Chuaria*	BP	237	N	N	-	N	Y
.	.	.	.	8	Small *Chuaria*	BP	237	N	N	-	N	Y
.	.	.	.	9	Small *Chuaria*	BP	237	N	N	-	N	Y
.	.	.	.	10	Small *Chuaria*	BP	237	N	N	-	N	Y
.	.	.	.	11	Small *Chuaria*	BP	238	N	N	-	N	Y
.	.	.	.	12	Small *Chuaria*	BP	238	N	N	-	N	Y
.	.	.	.	13	Small *Chuaria*	BP	238	N	N	-	N	Y
.	.	.	.	14	Small *Chuaria*	BP	238	N	N	-	N	Y
.	.	.	.	15	Small *Chuaria*	BP	238	N	N	-	N	Y
.	.	.	.	16	Small *Chuaria*	BP	238	N	N	-	N	Y
.	.	.	.	17	Small *Chuaria*	BP	239	N	N	-	N	Y
.	.	.	.	18	Small *Chuaria*	BP	239	N	N	-	N	Y
SFT-22.5-1	2009	Sifangtan	Argillaceous Dolostone	N/A	N/A	N/A	N	N	N	-	N	N
SFT-24-1	2009	Sifangtan	Argillaceous Dolostone	N/A	N/A	XS, BP	161, 208	N	N	-	N	N
.	.	.	.	1	Small *Chuaria*	BP	205	N	N	-	N	Y
.	.	.	.	2	Small *Chuaria*	BP	206	N	N	-	N	Y
.	.	.	.	3	Small *Chuaria*	BP	207	N	N	-	N	Y
.	.	.	.	4	Small *Chuaria*	BP	159, 160, 209	N	46, 48	-	N	Y
.	.	.	.	5	Small *Chuaria*	BP	209	N	N	-	N	Y
.	.	.	.	6	Small *Chuaria*	BP	159, 160, 209	47	43, 44, 45, 46	Mg, Si, O, Ca, C, Fe	Y	Y
.	.	.	.	7	Small *Chuaria*	BP	159, 160, 209	47	43, 44, 45, 46	Mg, Si, O, Ca, C, Fe	Y	Y
.	.	.	.	8	Small Chuaria	BP	209	N	N	-	N	N
SFT-24-2	2009	Sifangtan	Argillaceous Dolostone	N/A	N/A	N/A	N	N	N	-	N	N
SFT-24-3	2009	Sifangtan	Argillaceous Dolostone	N/A	N/A	N/A	N	N	N	-	N	N
.	.	.	.	1	Small *Chuaria*	BP	210	N	N	-	N	Y
.	.	.	.	2	Small *Chuaria*	BP	210	N	N	-	N	Y
.	.	.	.	3	Small *Chuaria*	BP	210	N	N	-	N	Y
.	.	.	.	4	Small *Chuaria*	BP	211	N	N	-	N	Y
.	.	.	.	5	Small *Chuaria*	BP	211	N	N	-	N	Y
.	.	.	.	6	Small *Chuaria*	BP	211	N	N	-	N	Y
.	.	.	.	7	Small *Chuaria*	BP	211	N	N	-	N	Y
.	.	.	.	8	Small *Chuaria*	BP	212	N	N	-	N	Y
.	.	.	.	9	Small *Chuaria*	BP	213	N	N	-	N	Y
.	.	.	.	10	Small *Chuaria*	BP	213	N	N	-	N	Y
.	.	.	.	11	Small *Chuaria*	BP	213	N	N	-	N	Y
.	.	.	.	12	Small *Chuaria*	BP	214	N	N	-	N	Y
.	.	.	.	13	Small *Chuaria*	BP	214	N	N	-	N	Y
.	.	.	.	14	Small *Chuaria*	BP	215	N	N	-	N	Y
.	.	.	.	15	Small *Chuaria*	BP	216	N	N	-	N	Y

.	.	.	.	16	Small *Chuaria*	BP	217	N	N	-	N	Y
.	.	.	.	17	Small *Chuaria*	BP	217	N	N	-	N	Y
.	.	.	.	18	Small *Chuaria*	BP	217	N	N	-	N	Y
.	.	.	.	19	Small *Chuaria*	BP	217	N	N	-	N	Y
.	.	.	.	20	Small *Chuaria*	BP	217	N	N	-	N	Y
.	.	.	.	21	Small *Chuaria*	BP	217	N	N	-	N	Y
SFT-24-4	2009	Sifangtan	Argillaceous Dolostone	N/A	N/A	N/A	N	N	N	-	N	N
.	.	.	.	1	Small *Chuaria*	BP	218	N	N	-	N	Y
.	.	.	.	2	Small *Chuaria*	BP	218	N	N	-	N	Y
.	.	.	.	3	Small *Chuaria*	BP	219	N	N	-	N	Y
.	.	.	.	4	Small *Chuaria*	BP	219	N	N	-	N	Y
.	.	.	.	5	Small *Chuaria*	BP	219	N	N	-	N	Y
SFT-24-5	2009	Sifangtan	Argillaceous Dolostone	N/A	N/A	N/A	N	N	N	-	N	N
SFT-24-6	2009	Sifangtan	Argillaceous Dolostone	N/A	N/A	N/A	N	N	N	-	N	N
SFT-24-7	2009	Sifangtan	Argillaceous Dolostone	N/A	N/A	BP	N	N	N	-	N	N
.	.	.	.	1	Small *Chuaria*	BP	220	N	N	-	N	Y
.	.	.	.	2	Small *Chuaria*	BP	221	N	N	-	N	Y
.	.	.	.	3	Small *Chuaria*	BP	221	N	N	-	N	Y
.	.	.	.	4	Small *Chuaria*	BP	222	N	N	-	N	Y
SFT-25.5	2009	Sifangtan	Argillaceous Dolostone	N/A	N/A	BP, XS	143, 144, 145	N	N	-	N	N
SFT-27-1	2009	Sifangtan	Argillaceous Dolostone	N/A	N/A	N/A	N	N	N	-	N	N
SFT-30.2-1	2009	Sifangtan	Argillaceous Dolostone	N/A	N/A	N/A	N	N	N	-	N	N
SFT-30.2-2	2009	Sifangtan	Argillaceous Dolostone	N/A	N/A	N/A	N	N	N	-	N	N
SFT-30.2-3	2009	Sifangtan	Argillaceous Dolostone	N/A	N/A	N/A	N	N	N	-	N	N
SFT-33.7	2009	Sifangtan	Argillaceous Dolostone	N/A	N/A	BP	246, 247	N	N	-	N	N
.	.	.	.	1	Small *Chuaria*	BP	223	N	N	-	N	Y
.	.	.	.	2	Small *Chuaria*	BP	224	N	N	-	N	Y
.	.	.	.	3	Small *Chuaria*	BP	224	N	N	-	N	Y
.	.	.	.	4	Small *Chuaria*	BP	225	N	N	-	N	Y
.	.	.	.	5	Small *Chuaria*	BP	225	N	N	-	N	Y
.	.	.	.	6	Small *Chuaria*	BP	226	N	N	-	N	Y
.	.	.	.	7	Small *Chuaria*	BP	227	N	N	-	N	Y
.	.	.	.	8	Small *Chuaria*	BP	227	N	N	-	N	Y
.	.	.	.	9	Small *Chuaria*	BP	227	N	N	-	N	Y
.	.	.	.	10	Small *Chuaria*	BP	227	N	N	-	N	Y
.	.	.	.	11	Small *Chuaria*	BP	227	N	N	-	N	Y
.	.	.	.	12	Small *Chuaria*	BP	228	N	N	-	N	Y
SFT-37	2009	Sifangtan	Argillaceous Dolostone	N/A	N/A	N/A	N	N	N	-	N	N

SFT-60-1	2009	Sifangtan	Argillaceous Dolostone	N/A	N/A	N/A	N	N	N	-	N	N
SFT-60-2	2009	Sifangtan	Argillaceous Dolostone	N/A	N/A	N/A	N	N	N	-	N	N
SFT-71	2009	Sifangtan	Argillaceous Dolostone	N/A	N/A	N/A	N	N	N	-	N	N
SFT-84	2009	Sifangtan	Argillaceous Dolostone	N/A	N/A	N/A	N	N	N	-	N	N
09-SX-DST-A1	2009	Sixi	Argillaceous Dolostone	N/A	N/A	N/A	N	N	N	-	N	N
09-SX-DST-A2	2009	Sixi	Argillaceous Dolostone	N/A	N/A	N/A	N	N	N	-	N	N
09-SX-DST-A3	2009	Sixi	Argillaceous Dolostone	N/A	N/A	N/A	N	N	N	-	N	N
09-SX-DST-A4	2009	Sixi	Argillaceous Dolostone	N/A	N/A	N/A	N	N	N	-	N	N
09-SX-DST-A5	2009	Sixi	Argillaceous Dolostone	N/A	N/A	BP	163	N	N	-	N	N
.	.	.	.	1	*Chuaria*	BP	164	N	N	-	Y	N
.	.	.	.	2	*Chuaria*	BP	164	N	N	-	Y	N
09-SX-DST-A6	2009	Sixi	Argillaceous Dolostone	N/A	N/A	N/A	N	N	N	-	N	N
.	.	.	.	1	*Chuaria*	XS	N	51	49, 50	Al, Mg, Si, O, Ca, C, P, S, Fe	N	N
09-SX-DST-A7	2009	Sixi	Argillaceous Dolostone	N/A	N/A	N/A	N	N	N	-	N	N
09-SX-DST-B	2009	Sixi	Argillaceous Dolostone	N/A	N/A	N/A	N	N	N	-	N	N
09-SX-DST-C	2009	Sixi	Argillaceous Dolostone	N/A	N/A	N/A	N	N	N	-	N	N
09-SX-DST-D	2009	Sixi	Argillaceous Dolostone	N/A	N/A	N/A	N	N	N	-	N	N
09-SX-DST-E1	2009	Sixi	Argillaceous Dolostone	N/A	N/A	N/A	N	N	N	-	N	N
09-SX-DST-E2	2009	Sixi	Argillaceous Dolostone	N/A	N/A	N/A	N	N	N	-	N	N
09-SX-DST-F	2009	Sixi	Highly Calcareous Siltstone	N/A	N/A	BP, XS	165, 166, 168, 169	N	N	-	N	N
.	.	.	.	1	*Chuaria*	BP	167	54	52, 53	Al, Mg, Si, O, Ca, C, S, Fe, K	Y	N
.	.	.	.	2	*Chuaria*	BP	167	57	55, 56	Al, Mg, Si, O, Ca, C, S, Fe, K	Y	N
09-SX-DST-G	2009	Sixi	Argillaceous Dolostone	N/A	N/A	N/A	N	N	N	-	N	N
09-SX-DST-H	2009	Sixi	Argillaceous Dolostone	N/A	N/A	N/A	N	N	N	-	N	N
09-SX-DST-I1	2009	Sixi	Argillaceous Dolostone	N/A	N/A	N/A	N	N	N	-	N	N
09-SX-DST-I2	2009	Sixi	Argillaceous Dolostone	N/A	N/A	N/A	N	N	N	-	N	N
09-SX-DST-I Chert	2009	Sixi	Argillaceous Dolostone	N/A	N/A	N/A	N	N	N	-	N	N
09-SX-DST-J1	2009	Sixi	Argillaceous Dolostone	N/A	N/A	BP	182, 183	N	N	-	N	N
09-SX-DST-J2	2009	Sixi	Argillaceous Dolostone	N/A	N/A	N/A	N	N	N	-	N	N
09-SX-DST-J3	2009	Sixi	Argillaceous Dolostone	N/A	N/A	N/A	N	N	N	-	N	N
09-SX-DST-J4	2009	Sixi	Argillaceous Dolostone	N/A	N/A	N/A	N	N	N	-	N	N

MH-1	2009	Miaohe	Limestone/Siltstone	N/A	N/A	N/A	N	N	N	-	N	N
MH-2	2009	Miaohe	Limestone/Siltstone	N/A	N/A	N/A	N	N	N	-	N	N
MH-3	2009	Miaohe	Limestone/Siltstone	N/A	N/A	N/A	N	N	N	-	N	N
MH-4	2009	Miaohe	Limestone/Siltstone	N/A	N/A	N/A	N	N	N	-	N	N
MH-5	2009	Miaohe	Limestone/Siltstone	N/A	N/A	N/A	N	N	N	-	N	N
MH-6	2009	Miaohe	Limestone/Siltstone	N/A	N/A	BP	268	N	N	-	N	N
MH-7	2009	Miaohe	Limestone/Siltstone	N/A	N/A	BP, XS	146, 147, 148, 149, 150, 151	N	N	-	N	N
.	.	.	.	1	*Vendotaenia*	BP	149, 157, 158	59, 61	58, 60	Al, Mg, Si, O, Ca, C, S, Fe	Y	N
MH-8	2009	Miaohe	Limestone/Siltstone	N/A	N/A	N/A	N	N	N	-	N	N
03-WH-1	2003	Wuhe	Limestone/Siltstone	N/A	N/A	XS	N	N	62, 63	-	N	N
.	.	.	.	1	*Vendotaenia*	XS	253, 254	66	64, 65	Mg, O, Ca, C, S, K	N	N
.	.	.	.	2	*Vendotaenia*	XS	255, 256	N	N	-	N	N
.	.	.	.	3	*Vendotaenia*	XS	257	N	N	-	N	N

Table A2. Axes length measurements for *Chuaria* and small *Chuaria* used for population analysis.

Locality	Taxon	Axis 1 (mm)	Axis 2 (mm)
Sixi	*Chuaria*	1.7	1.7
		2.3	2
		0.65	0.5
		N/A	1.3
		2.1	1.6
		2.15	1.5
		2.75	2.15
		1.8	1.7
		0.6	N/A
		1.725	0.975
		1	1
		0.65	0.625
		1.05	0.8
		0.85	0.625
		1.05	0.8
		2.775	1.75
		1.8	0.95
		1.05	0.95
		1.2	1
		1.8	1.2
		2.2	1.65
		N/A	1.45
		1.15	0.7
		0.975	0.65
		N/A	0.45
		1.85	1
		1.2	N/A
		0.975	0.975
		1.625	1.45

	Tawuia	2.375	1.55
		3.85	1.85
		1.95	0.925
Jiulongwan (lower Member II)	*Chuaria*	1.25	1
		1.45	0.85
		4.3	3
		4.25	2.7
		6.15	5
		3.95	2.55
		2	1.65
		4.25	3.15
		2.05	1.9
		0.65	0.5
		4.4	3
		N/A	1.5
		2	1.95
		2.75	2.35
		1.25	1.1
		1.95	1.35
		1.45	0.9
		1.35	0.95
		1.8	1.3
		2.35	2.1
		1.375	1.35
		1	0.75
		0.6	0.45
		1.85	1.2
		0.85	0.75
		0.85	0.6
		0.55	0.5
		0.3	0.3

		1.3	N/A
		1	0.75
		1.3	1.05
		0.75	0.4
		1.7	1.2
		1.15	0.75
		1.1	0.85
		1.15	0.925
		0.9	0.75
		1.2	0.85
		1.45	1.15
		1.3	0.725
		0.9	0.7
		1	0.8
		1.25	0.8
		2.15	1.5
		0.9	0.8
		1.85	2.75
		0.8	0.85
		1.55	1.8
		1.4	1.2
		1.2	1.1
		1.15	1.4
		2	1.9
		1.5	1.05
		1.8	1.45
		1.1	1.05
		1.05	1
		1.625	1.4
		1.1	0.95
	Tawuia	8.15	5.45
		3.9	1.3
		2.6	9.8

		4	11.55
		N/A	5
		4.05	1.6
Sifangtan and Jiulongwan (upper Member II)	small *Chuaria*	0.88	0.57
		0.55	0.53
		0.68	0.52
		0.69	0.53
		0.69	0.62
		0.76	0.54
		0.67	0.65
		0.74	0.65
		0.74	0.57
		0.71	0.59
		0.61	0.61
		0.7	0.59
		0.65	0.64
		1.05	0.74
		0.63	0.57
		0.91	0.46
		0.6	0.55
		1.2	0.68
		0.7	0.6
		0.61	0.44
		1	0.76
		0.72	0.7
		0.85	0.73
		0.77	0.69
		0.8	0.72
		0.65	0.54

		0.73	0.49
		0.55	0.51
		0.46	0.46
		0.49	0.43
		1	0.93
		0.92	0.74
		0.68	0.59
		0.67	0.63
		0.73	0.69
		0.89	0.71
		0.78	0.61
		0.5	0.46
		0.62	0.51
		0.78	0.67
		0.42	0.37
		0.69	0.6
		0.62	0.56
		0.67	0.58
		0.7	0.46
		0.49	0.44
		0.6	0.54
		0.65	0.59
		0.64	0.55
		0.3	0.27
		0.29	0.26
		0.47	0.46
		0.54	0.49
		0.66	0.63
		0.44	0.37
		0.64	0.59
		0.31	0.22
		0.66	0.6
		0.52	0.4
		0.67	0.54

		0.66	0.51
		0.59	0.51
		0.75	0.66
		0.72	0.72
		0.89	0.83
		0.87	0.87
		0.81	0.76
		0.88	0.71
		0.425	0.575
		0.725	0.55
		0.675	0.55
		0.7	0.55
		0.7	0.7
		0.65	0.65
		1	0.675
		0.65	0.55
		0.7	0.625
		0.9	0.825
		0.9	0.8
		0.9	0.8
		0.75	0.675
		0.725	0.625
		0.675	0.6
		1	0.85
		0.8	0.575
		0.95	0.825
		0.9	0.8
		0.65	0.45
		0.875	0.85
		0.9	0.8
		0.825	0.825
		0.6	0.575